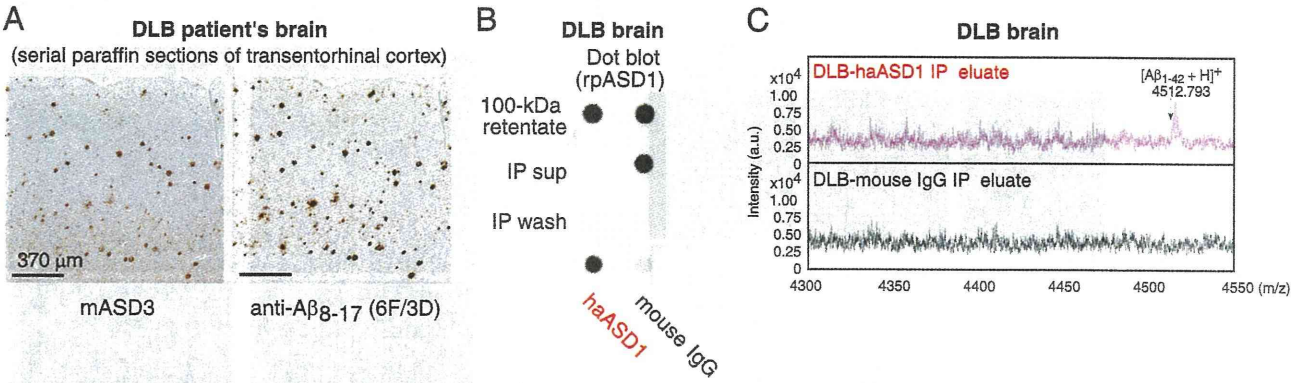

FIGURE 3. **Native ASPDs exist in DLB brains.** *A*, immunostaining using mASD3 (2.5 μg/ml) and anti-Aβ8–17 (pretreated with formic acid; 1:100; DAKO). *B*, IP was performed with haASD1 or mouse IgG as in Fig. 2*F* using 100-kDa retentates (4 μg of soluble brain extracts/IP). Dot blotting (0.04 μg/ml rpASD1) of 100-kDa retentates (2 μg of soluble brain extracts/dot), IP supernatants (*sup*), wash, and eluate is shown. *C*, representative MALDI-TOF/MS data.

recognition of different epitopes (Table 1). Judging from the results of quantification of dot blots using rpASD1 (Fig. 2*G*), we obtained about 43 pmol of native ASPDs (expressed as Aβ monomer concentration) from 1 g of AD brain tissues ($n = 6$). The rpASD1 reactivity in the IP eluates was considered to be mostly due to the 10–15-nm spheres, because the number of spheres counted by TEM (Fig. 2*H*) (1.0×10^{10} 10–15-nm sphere/μl estimated from the number of spheres in Fig. 2*K*, $n = 6$) was very similar to the amount of rpASD1-reactive ASPD obtained from dot blots (1.1×10^{10} native ASPD/μl based on the ASPD concentration in Fig. 2*K*, $n = 8$). This means that rpASD1-reactive 10–15-nm spheres were selectively isolated by a combination of 100-kDa retention and IP. Indeed, as shown by the TEM data (Fig. 2*H*), the non-ASPD small-sized spheres (<10 nm) that had been present in large amounts in 100-kDa retentates of AD and NCI were largely eliminated by the IP procedure (compare Fig. 2, *I* with *E*). Accordingly, we successfully isolated native ASPDs, consisting of 10–15-nm spheres (>95%; Fig. 2, *H* and *I*), from 100-kDa retentates of AD. In contrast, native ASPD-like assemblies were scarcely detected in IP eluates from 100-kDa retentates of NCI (Fig. 2, *G* and *K*). We next examined whether native ASPDs consisted of Aβ. Mass spectrometric analysis showed that singly charged ions corresponding to Aβ-(1–42) and Aβ-(1–40) were detected in native ASPDs (Fig. 2*J*). These results collectively demonstrate that 10–15-nm spherical Aβ assemblies isolated from AD brains are native ASPDs. Notably, anti-pan Aβ 6E10 could not immunoisolate native ASPDs (data not shown), probably because of its weak affinity for ASPDs ($K_d \approx 10^{-9}$ M) compared with ASD antibodies ($K_d < 10^{-12}$ M) (Table 1). We also confirmed that anti-pan oligomer A11 antibody failed to detect native ASPDs (supplemental Fig. S4).

Having isolated native ASPDs selectively from human AD brains, we next examined whether they elicited neurodegeneration of rat primary neuronal cells. Surprisingly, AD-derived native ASPDs were even more toxic than synthetic ASPDs (Fig. 2*K*). These results collectively demonstrate that we have newly isolated A11-negative, high mass assemblies that cause neuronal cell death and that differ in mass and surface tertiary structure from other reported nonfibrillar Aβ assemblies.

Native ASPD Amount Correlates with the Pathologic Severity of AD—We next examined whether the amount of native ASPD correlated with the pathologic severity of AD brains. Larger amounts of native ASPD were present in AD patients with severe pathology (diagnosed "C" according to the CERAD criteria (43)) than in AD patients with moderate pathology (diagnosed "B") (Fig. 2*C*). Furthermore, in AD patients with severe pathology, significantly higher amounts of native ASPD were detected in the frontal or temporal cortices (7.2 ± 1.5 nmol/g brain tissue, $n = 3$, Scheffé post hoc test $p = 0.0012$) than in the cerebellum (0.14 ± 0.1 nmol/g brain tissue). The result is consistent with previous findings that the cerebellum in AD is pathologically less affected (44, 45).

The above observations suggest the involvement of native ASPDs in neurodegeneration of AD brains. We therefore examined brains of patients suffering from DLB, the second most frequent cause of cognitive decline associated with neurodegeneration in the elderly (46, 47), because the majority of DLB brains have been shown to have AD-type pathology, including plaques (46–48). Interestingly, native ASPDs were also isolated from DLB brains (Fig. 3, *A–C*).

AD-derived Native ASPDs Cause Severe Degeneration of Human Neuronal Cells—To further elucidate the relationship between neuronal loss and native ASPDs, we first examined whether native ASPDs induce degeneration of human mature neuronal cells. Because studies using human primary neurons are problematic for ethical and practical reasons, cells with neuronal properties were induced from human bone marrow stromal cells (MSCs) (49). Initially, postmitotic neuronal cells were induced from human MSCs (>95% were neuron-specific MAP2ab-positive cells without glia) (49). Treatment of these cells with glial cell line-derived neurotrophic factor promoted their maturation into functional neuronal cells (49). We found that a 2-day treatment of the human MSC-derived functional neuronal cells with isolated native ASPDs caused severe degeneration, whereas IP eluates from NCI brains had no effect (Fig. 4*A*). In addition, pretreatment with mASD3 antibody (100 μg/ml) significantly blocked this toxicity (Fig. 4*A*), as observed in the case of the 158–669-kDa ASPDs (supplemental Fig. S5*A*), dem-

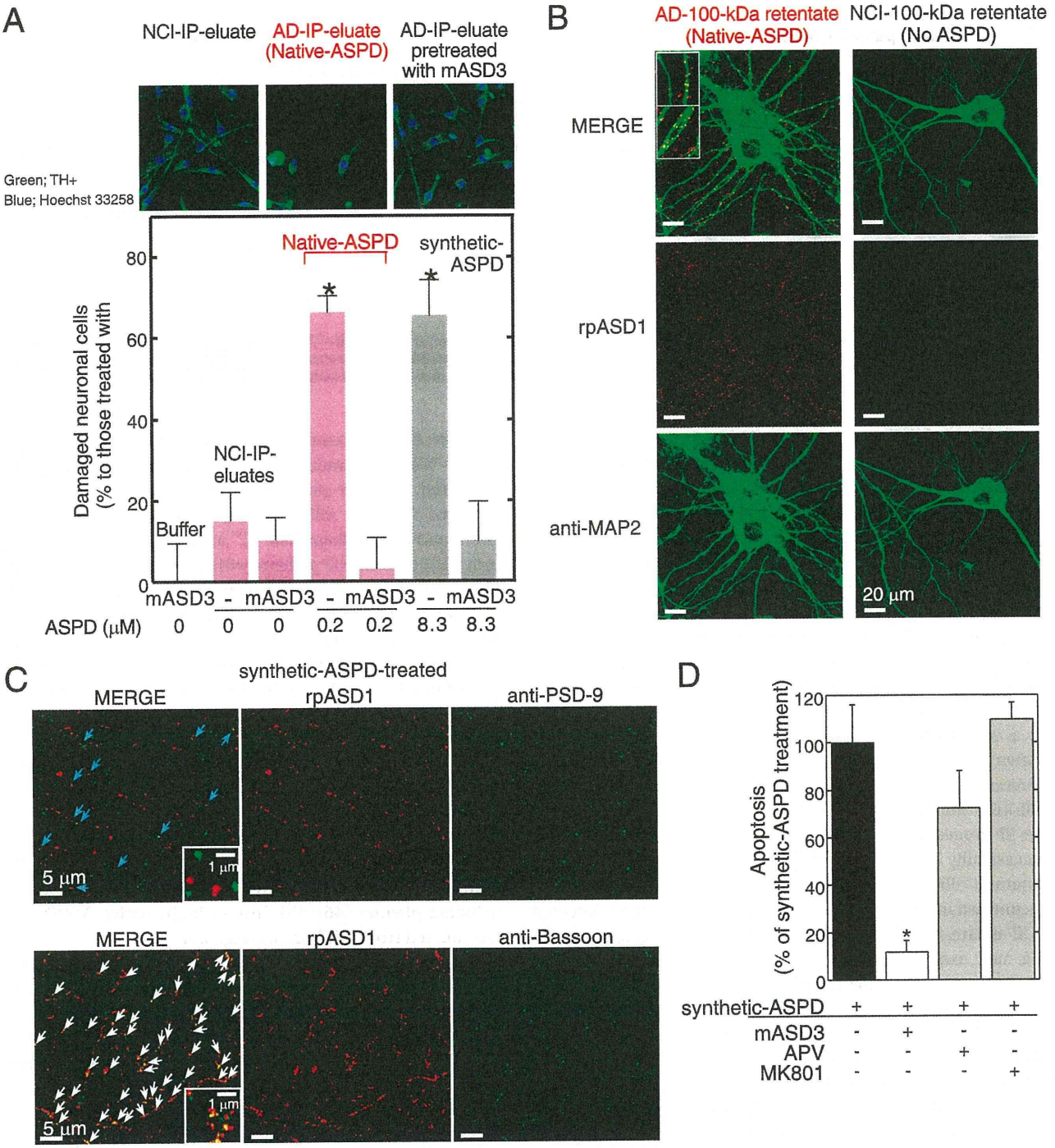

FIGURE 4. **Characterization of native and synthetic ASPD-induced toxicity.** *A*, IP was performed using haASD1 as in Fig. 2*F*. Human neuronal cells were treated for 2 days with AD or NCI-IP eluates, with or without 2-h mASD3 (100 μg/ml) pretreatment. Nondamaged cells were counted after tyrosine hydroxylase (*TH*+) and Hoechst 33258 staining. The ratio of damaged cells to neuronal cells treated with buffer alone (mean ± S.D.) is shown (Scheffé post hoc test; *, $p < 0.0001$, $n = 5$). Neuronal cells treated with mASD3 alone or NCI-IP eluates showed only background levels of damaged cells similar to those in the case of cells treated with buffer. *B* and *C*, mature rat hippocampal neurons (24 DIV in *B* and 19 DIV in *C*) were incubated for 30 min either with 100-kDa retentates of AD (containing 0.8 μM native ASPDs) or NCI (no native ASPD detected) brain extracts in *B* or with 0.5 μM 158–669-kDa ASPDs (prepared from Aβ-(1–42); see Fig. 1*A*) in *C*. Bound ASPDs were detected by rpASD1, as in Fig. 1*D*. Punctate labeling was found primarily on neurites and surrounding cell bodies of neurons treated with native or synthetic ASPDs, but it was hardly detectable in neurons treated with the NCI retentates. A representative high power view is shown in the *inset* (*B*; *bar*, 5 μm). Neurons were co-stained with an antibody against anti-MAP2 in *B*, against a postsynaptic marker PSD-95 in *C* (*upper panels*), or against a presynaptic marker bassoon in *C* (*lower panels*). Z-stack images are shown (except *lower panels* in *C*) as in Fig. 1*D*. Bound ASPDs did not co-localize with PSD-95 but were concentrated with bassoon (*white arrows* in *C*), although they were occasionally localized in close proximity to PSD-95 (*blue arrows* in *C*). *D*, mature rat hippocampal neurons (21 DIV) were treated with 1 μM 158–669-kDa ASPDs for 2 days, with or without pretreatment (100 μg/ml mASD3 for 2 h; competitive (APV) or uncompetitive (MK801) NMDA-R antagonists (10 μM) for 30 min). Data represent mean ± S.D. (Scheffé post hoc test; *, $p = 0.0039$, compared with synthetic ASPDs; synthetic ASPDs, $n = 7$; synthetic ASPDs + APV or MK801, $n = 5$; synthetic ASPDs + mASD3, $n = 4$).

onstrating that the observed neuronal cell death was caused by native ASPDs.

We then examined whether native ASPDs bind mature rat hippocampal neurons, as is observed in the case of synthetic ASPDs (Fig. 1*D* and supplemental Fig. S5*B*). Binding of AD-derived native ASPDs to 24-DIV mature rat hippocampal neurons was detected with rpASD1 most intensely in neurites and also to some extent in cell bodies (Fig. 4*B*). These results suggest that, despite the difference in dose dependence of neurotoxicity (Figs. 2*K* and 4*A*), native and synthetic ASPDs share essentially the same mechanism of neurotoxicity, *i.e.* they have the same surface tertiary structure that is responsible for exerting the toxicity. We speculate that the apparent difference in dose dependence might be attributed to differences in molecular compositions, but testing this idea will require further analyses using large amounts of isolated native ASPDs.

Mode of Native ASPD Neurotoxicity Is Different from That of Other Reported Aβ Assemblies—The above results (Fig. 4, *A* and *B*) show that native ASPDs cause neuronal cell death, possibly by binding to neuronal cell surfaces. We therefore examined ASPD-binding sites on mature neurons to elucidate the molecular basis of native ASPD neurotoxicity. As shown in the high power images in Fig. 4*B* (*inset*), bound native ASPDs appeared to protrude from the MAP2 staining of dendrites. Essentially the same results were obtained with the binding of synthetic ASPDs (supplemental Fig. S5*B* (*inset*)). Because of the limited availability of native ASPDs, we employed synthetic ASPDs for further analysis, as synthetic and native ASPDs share essential properties. Consistent with the above observation, the binding of synthetic ASPDs did not co-localize with a postsynaptic marker, PSD-95 (Fig. 4*C*, *upper panel*), although it was occasionally detected in close proximity to PSD-95 (*blue arrows* in *C*). Instead, ASPD-binding sites appeared to be concentrated at presynaptic sites stained by the antibody against a presynaptic marker, bassoon (*white arrows* in Fig. 4*C*, *lower panel*).

Although previous studies using cell or slice culture systems have found that Aβ assemblies such as dimers, ADDLs and AβOs bind postsynapses and depend on postsynaptic signaling mechanisms for exerting synaptotoxicity (23), the presynaptic binding of ASPDs apparent in Fig. 4*B* suggests that ASPD neurotoxicity would not require postsynaptic signaling mechanisms such as the *N*-methyl-D-aspartate glutamate receptor (NMDA-R) pathway. Indeed, neither a competitive (APV) nor an uncompetitive (MK801) NMDA-R antagonist inhibited synthetic ASPD-induced neurodegeneration (Fig. 4*D*). As noted above, native and synthetic ASPDs share the common surface tertiary structure responsible for exerting the toxicity. Therefore, the findings obtained with synthetic ASPDs (Fig. 4, *C* and *D*) strongly suggest that native ASPDs cause neuronal cell death through presynaptic target(s) on mature neurons. Furthermore, these observations are consistent with the findings indicating that native ASPDs have a distinct surface tertiary structure from other reported Aβ assemblies and support the hypothesis that native ASPDs have a different target(s) from other Aβ assemblies.

DISCUSSION

Aβ assemblies are considered to acquire surface tertiary structures that are not present in physiologic Aβ monomers and that induce synaptic impairment and neuronal loss through interactions with neuronal cells. Therefore, as recently suggested (12), it is reasonable to classify seemingly different Aβ assemblies in terms of their immunoreactivity to antibodies that recognize particular surface tertiary structure. Because the surface tertiary structure mediates the binding of Aβ assemblies to their target(s) and is therefore responsible for exerting the toxic effects, Aβ assemblies having distinct surface tertiary structures are likely to have distinct mechanisms of neurotoxicity and may contribute differently to the disease development. Here we have demonstrated the existence of patient-derived native ASPDs by selectively immunoisolating them from AD and DLB brains (Figs. 2 and 3) using ASPD tertiary structure-dependent antibodies (Fig. 1 and Table 1). The native ASPDs (>100 kDa) thus obtained are larger in mass than AD-derived Aβ dimers and other reported assemblies such as 12-mers (53~60 kDa; ADDLs, globulomer, Aβ*56) or AβOs (~90 kDa) (supplemental Table S1). More importantly, native ASPDs are considered to have a distinct surface tertiary structure from those other assemblies because they differ in immunospecificity, as illustrated by the fact that ASPD tertiary structure-dependent antibodies showed minimal reactivity with the 100-kDa filtrate containing monomers and dimers (Fig. 1*A*) or with ADDLs (supplemental Fig. S1*A*) (16) in dot blots. Additionally, anti-pan oligomer A11 antibody (22) recognized AβOs but not synthetic ASPDs (Fig. 1*B*) or native ASPDs (supplemental Fig. S4). Finally, anti-Aβ N-terminal antibodies such as 82E1 blocked the synaptotoxicity of AD-derived dimers (30) but failed to block synthetic ASPD-induced neurodegeneration (supplemental Fig. S5*A*). These results all indicate a difference in the surface tertiary structure between these assemblies and ASPDs.

As for the cellular basis of the Aβ-induced synaptic changes, previous studies have suggested the involvement of postsynaptic signaling mechanisms (23). For example, the binding of ADDLs and AβOs has been reported to co-localize with PSD-95 (19, 23). As expected from the postsynaptic locale of their binding, ADDLs bind close to or at NMDA-R (23), and NMDA-R antagonists inhibit ADDL-induced dendritic changes (23), reactive oxygen species formation (50), and insulin receptor impairment (51). NMDA-R antagonists have also been reported to inhibit Aβ dimer-induced synaptic loss (24, 30). Interestingly, cellular prion protein, which interacts with NMDA-R (52), has recently been reported to serve as a high affinity postsynaptic receptor mediating ADDL-induced synaptic dysfunction (53). Taken together, these studies are consistent with the idea that Aβ dimers, ADDLs, and AβOs perturb postsynaptic transmission (19, 23, 30).

We found that, unlike the above Aβ assemblies, ASPDs bind presynaptic target(s) on neurons to induce neurodegeneration (Fig. 4, *A–C*). This may be reasonable in view of the distinct ASPD surface tertiary structure. Although the actual targets of native ASPDs remain to be elucidated, native ASPDs seem to affect mature neuron-specific molecules or cellular pathways,

as synthetic ASPD-induced neurotoxicity appeared to be confined to neurons, being especially active toward mature neurons, but sparing non-neuronal cells and immature neurons (supplemental Fig. S6, *A–C*). Together, the findings indicate that native ASPDs are patient-derived, A11-negative, high mass Aβ assemblies with a distinct toxic surface that binds presynaptic target(s) on mature neurons, leading to neuronal loss (supplemental Table S1). Although further studies are required to reveal how native ASPDs exert neurotoxicity in the brains of patients with AD, our findings indicate for the first time that presynaptic signaling mechanisms may play a critical role in Aβ-induced neurodegeneration in AD.

Recent *in vivo* as well as *in vitro* studies support the toxicity of nonfibrillar Aβ assemblies and their possible causative roles in the neuropathology of AD (54–56), which is consistent with the dissociation between fibril load and cognitive decline in patients with AD (32, 57, 58). Thus, Aβ assemblies other than fibrils have been considered to be the preferred therapeutic targets for AD (54). However, the nature of the Aβ species and the oligomer state responsible for the pathogenesis remain controversial because of the heterogeneity of Aβ assemblies in terms of Aβ species and oligomer size. It is also unknown how Aβ monomers assemble into oligomers in living human brains. Nevertheless, previous *in vitro* studies have shown that Aβ monomers develop into a variety of assemblies that might represent distinct structural variants (10–13). These studies suggest that assembly may not be a linear process but may be the result of a series of multiple processes involving intermediates from side paths. Taking all the results together, it seems reasonable to assume that the brains of patients with AD contain distinct types of Aβ assemblies with different surface tertiary structures that may play different roles in AD development. Therefore, identification and characterization of all types of Aβ assemblies actually present in brains from humans with AD will be important for understanding the molecular mechanisms underlying the AD progression from the initial step to the symptomatic phase and for the development of therapies based on this understanding. Fractionation studies using oligomer tertiary structure-dependent antibodies as shown here will help to elucidate the assembly process and to determine the Aβ assembly state causing the pathogenesis. We have isolated native ASPDs that cause degeneration of mature human neuronal cells *in vitro* (Fig. 4*A*) and have shown that the amount of native ASPD is correlated with the pathologic severity of clinically proven AD cases (Fig. 2*C*).

These findings suggest that native ASPDs might be a candidate for Aβ assemblies that directly cause neuronal loss in the brains of humans with AD. However, it remains to be elucidated whether or not ASPDs play a particular role in the onset or early stage of disease development. Braak and coworkers (59) have compared the expansion of Aβ pathology in whole brain regions between AD cases and nondemented cases with or without Aβ-related pathology. They found that patients with clinically proven AD exhibit late Aβ stages, although the nondemented cases with AD-related pathology show early Aβ stages. Their findings suggest that AD brains develop pathologic Aβ deposition before clinical symptoms become apparent, and this may start much earlier in nondemented patients with AD-related Aβ pathology. Quantitative studies, with the assistance of clinicians, on the brains of people in different Aβ stages, including nondemented people with AD-related Aβ pathology, will be helpful to elucidate if ASPDs play a role in neuronal loss in AD from the early stage of disease development.

Analyses on brains of APP-transgenic mice with or without neuronal loss would also help to elucidate the relationship between ASPDs and neuronal loss. Although the strain does not show neuronal loss, we examined *Tg2576* mice, the most widely used AD-model mice carrying the human Swedish APP mutant (60), by means of immunohistochemistry and IP. ASPD-like assemblies were only minimally detected in the cerebral cortex of *Tg2576* mice (supplemental Fig. S7, *A* and *B*);: they were not detected up to 14 months and only a very small amount (~0.01 nmol/mg extracts) was detected at 23 months. As previously reported (18, 61), other Aβ assemblies such as dimers and Aβ*56 were increased in *Tg2576* mice, and total Aβ reached levels comparable with those in human AD (supplemental Fig. S7*C*). With respect to mice with neuronal loss, in addition to certain APP transgenic mice (28, 29), there is a growing number of other AD-model mice, which have been produced by combining APP mutations with either presenilin-1 mutations (62, 63), Tau protein mutations (64), or nitric-oxide synthase knock-out (65). It should be noted that the mouse is not a perfect model of human AD, but these mice are considered to more closely resemble what occurs in the human brains. Therefore, further analysis to examine whether ASPD-like assemblies are present in these mice, which do show massive neuronal loss, will contribute to establish the relationship between neuronal loss and ASPDs.

In addition to the above, we are currently seeking to establish a direct link between native ASPDs and neuronal loss in brains from humans with AD by searching for the toxic target(s) of ASPDs on mature neurons. The identification of native ASPDs and availability of the toxicity-neutralizing antibodies should facilitate a mechanistic understanding of the cellular basis of neuronal cell loss in AD, as well as the development of therapies based on this understanding.

Acknowledgments—We thank Drs. George R. Martin, Takaomi C. Saido, Sangram S. Sisodia, R. Yu, Y. Fukazawa, D. Masui, M. Hoshino, H. Hara, and A. Sakai, for critical discussions; Dr. Charles G. Glabe for providing control blots for A11 antibody through Invitrogen; and Drs. T. Nirasawa, S. Horie, H. Kinoshita, S. Miyama, Y. Ogawa, and N. Takino for technical assistance.

REFERENCES

1. Ross, C. A., and Poirier, M. A. (2005) *Nat. Rev. Mol. Cell Biol.* **6,** 891–898
2. Selkoe, D. J. (1991) *Neuron* **6,** 487–498
3. Lansbury, P. T., and Lashuel, H. A. (2006) *Nature* **443,** 774–779
4. Iwatsubo, T. (2007) *Neuropathology* **27,** 474–478
5. Soto, C., and Estrada, L. D. (2008) *Arch. Neurol.* **65,** 184–189
6. Chiti, F., and Dobson, C. M. (2009) *Nat. Chem. Biol.* **5,** 15–22
7. Hardy, J., and Selkoe, D. J. (2002) *Science* **297,** 353–356
8. Tanzi, R. E., and Bertram, L. (2005) *Cell* **120,** 545–555
9. Saido, T. C., and Iwata, N. (2006) *Neurosci. Res.* **54,** 235–253
10. Klein, W. L., Stine, W. B., Jr., and Teplow, D. B. (2004) *Neurobiol. Aging* **25,** 569–580

11. Walsh, D. M., and Selkoe, D. J. (2007) *J. Neurochem.* **101,** 1172–1184
12. Glabe, C. G. (2008) *J. Biol. Chem.* **283,** 29639–29643
13. Roychaudhuri, R., Yang, M., Hoshi, M. M., and Teplow, D. B. (2009) *J. Biol. Chem.* **284,** 4749–4753
14. Walsh, D. M., Lomakin, A., Benedek, G. B., Condron, M. M., and Teplow, D. B. (1997) *J. Biol. Chem.* **272,** 22364–22372
15. Podlisny, M. B., Ostaszewski, B. L., Squazzo, S. L., Koo, E. H., Rydell, R. E., Teplow, D. B., and Selkoe, D. J. (1995) *J. Biol. Chem.* **270,** 9564–9570
16. Lambert, M. P., Barlow, A. K., Chromy, B. A., Edwards, C., Freed, R., Liosatos, M., Morgan, T. E., Rozovsky, I., Trommer, B., Viola, K. L., Wals, P., Zhang, C., Finch, C. E., Krafft, G. A., and Klein, W. L. (1998) *Proc. Natl. Acad. Sci. U.S.A.* **95,** 6448–6453
17. Barghorn, S., Nimmrich, V., Striebinger, A., Krantz, C., Keller, P., Janson, B., Bahr, M., Schmidt, M., Bitner, R. S., Harlan, J., Barlow, E., Ebert, U., and Hillen, H. (2005) *J. Neurochem.* **95,** 834–847
18. Lesné, S., Koh, M. T., Kotilinek, L., Kayed, R., Glabe, C. G., Yang, A., Gallagher, M., and Ashe, K. H. (2006) *Nature* **440,** 352–357
19. Deshpande, A., Mina, E., Glabe, C., and Busciglio, J. (2006) *J. Neurosci.* **26,** 6011–6018
20. Chimon, S., Shaibat, M. A., Jones, C. R., Calero, D. C., Aizezi, B., and Ishii, Y. (2007) *Nat. Struct. Mol. Biol.* **14,** 1157–1164
21. Lacor, P. N., Buniel, M. C., Chang, L., Fernandez, S. J., Gong, Y., Viola, K. L., Lambert, M. P., Velasco, P. T., Bigio, E. H., Finch, C. E., Krafft, G. A., and Klein, W. L. (2004) *J. Neurosci.* **24,** 10191–10200
22. Kayed, R., Head, E., Thompson, J. L., McIntire, T. M., Milton, S. C., Cotman, C. W., and Glabe, C. G. (2003) *Science* **300,** 486–489
23. Lacor, P. N., Buniel, M. C., Furlow, P. W., Clemente, A. S., Velasco, P. T., Wood, M., Viola, K. L., and Klein, W. L. (2007) *J. Neurosci.* **27,** 796–807
24. Shankar, G. M., Bloodgood, B. L., Townsend, M., Walsh, D. M., Selkoe, D. J., and Sabatini, B. L. (2007) *J. Neurosci.* **27,** 2866–2875
25. Cleary, J. P., Walsh, D. M., Hofmeister, J. J., Shankar, G. M., Kuskowski, M. A., Selkoe, D. J., and Ashe, K. H. (2005) *Nat. Neurosci.* **8,** 79–84
26. Ashe, K. H. (2001) *Learn Mem.* **8,** 301–308
27. Hock, B. J., Jr., and Lamb, B. T. (2001) *Trends Genet.* **17,** S7–S12
28. Calhoun, M. E., Wiederhold, K. H., Abramowski, D., Phinney, A. L., Probst, A., Sturchler-Pierrat, C., Staufenbiel, M., Sommer, B., and Jucker, M. (1998) *Nature* **395,** 755–756
29. Bondolfi, L., Calhoun, M., Ermini, F., Kuhn, H. G., Wiederhold, K. H., Walker, L., Staufenbiel, M., and Jucker, M. (2002) *J. Neurosci.* **22,** 515–522
30. Shankar, G. M., Li, S., Mehta, T. H., Garcia-Munoz, A., Shepardson, N. E., Smith, I., Brett, F. M., Farrell, M. A., Rowan, M. J., Lemere, C. A., Regan, C. M., Walsh, D. M., Sabatini, B. L., and Selkoe, D. J. (2008) *Nat. Med.* **14,** 837–842
31. Kuo, Y. M., Emmerling, M. R., Vigo-Pelfrey, C., Kasunic, T. C., Kirkpatrick, J. B., Murdoch, G. H., Ball, M. J., and Roher, A. E. (1996) *J. Biol. Chem.* **271,** 4077–4081
32. Lue, L. F., Kuo, Y. M., Roher, A. E., Brachova, L., Shen, Y., Sue, L., Beach, T., Kurth, J. H., Rydel, R. E., and Rogers, J. (1999) *Am. J. Pathol.* **155,** 853–862
33. McLean, C. A., Cherny, R. A., Fraser, F. W., Fuller, S. J., Smith, M. J., Beyreuther, K., Bush, A. I., and Masters, C. L. (1999) *Ann. Neurol.* **46,** 860–866
34. Gómez-Isla, T., Hollister, R., West, H., Mui, S., Growdon, J. H., Petersen, R. C., Parisi, J. E., and Hyman, B. T. (1997) *Ann. Neurol.* **41,** 17–24
35. Morrison, J. H., and Hof, P. R. (1997) *Science* **278,** 412–419
36. Larrieu, S., Letenneur, L., Orgogozo, J. M., Fabrigoule, C., Amieva, H., Le Carret, N., Barberger-Gateau, P., and Dartigues, J. F. (2002) *Neurology* **59,** 1594–1599
37. Bouwman, F. H., Schoonenboom, S. N., van der Flier, W. M., van Elk, E. J., Kok, A., Barkhof, F., Blankenstein, M. A., and Scheltens, P. (2007) *Neurobiol. Aging* **28,** 1070–1074
38. Hoshi, M., Sato, M., Matsumoto, S., Noguchi, A., Yasutake, K., Yoshida, N., and Sato, K. (2003) *Proc. Natl. Acad. Sci. U.S.A.* **100,** 6370–6375
39. Lomakin, A., Chung, D. S., Benedek, G. B., Kirschner, D. A., and Teplow, D. B. (1996) *Proc. Natl. Acad. Sci. U.S.A.* **93,** 1125–1129
40. Demuro, A., Mina, E., Kayed, R., Milton, S. C., Parker, I., and Glabe, C. G. (2005) *J. Biol. Chem.* **280,** 17294–17300
41. Kuwano, R., Miyashita, A., Arai, H., Asada, T., Imagawa, M., Shoji, M., Higuchi, S., Urakami, K., Kakita, A., Takahashi, H., Tsukie, T., Toyabe, S., Akazawa, K., Kanazawa, I., and Ihara, Y. (2006) *Hum. Mol. Genet.* **15,** 2170–2182
42. Kayed, R., Head, E., Sarsoza, F., Saing, T., Cotman, C. W., Necula, M., Margol, L., Wu, J., Breydo, L., Thompson, J. L., Rasool, S., Gurlo, T., Butler, P., and Glabe, C. G. (2007) *Mol. Neurodegener.* **2,** 18
43. Mirra, S. S., Heyman, A., McKeel, D., Sumi, S. M., Crain, B. J., Brownlee, L. M., Vogel, F. S., Hughes, J. P., van Belle, G., and Berg, L. (1991) *Neurology* **41,** 479–486
44. Li, Y. T., Woodruff-Pak, D. S., and Trojanowski, J. Q. (1994) *Neurobiol. Aging* **15,** 1–9
45. Kepe, V., Huang, S. C., Small, G. W., Satyamurthy, N., and Barrio, J. R. (2006) *Methods Enzymol.* **412,** 144–160
46. Ince, P. G., and McKeith, I. G. (2003) in *Neurodegeneration: The Molecular Pathology of Dementia and Movement Disorders* (Dickson, D., ed) pp. 188–197, ISN Neuropath Press, Basel
47. Giasson, B. I., Lee, V. M.-Y., and Trojanowski, J. Q. (2004) in *The Neuropathology of Dementia* (Esiri, M., Lee, V. M.-Y., and Trojanowski, J. Q., eds) 2nd Ed., pp. 353–375, Cambridge University Press, Cambridge
48. Kosaka, K. (1990) *J. Neurol.* **237,** 197–204
49. Dezawa, M., Kanno, H., Hoshino, M., Cho, H., Matsumoto, N., Itokazu, Y., Tajima, N., Yamada, H., Sawada, H., Ishikawa, H., Mimura, T., Kitada, M., Suzuki, Y., and Ide, C. (2004) *J. Clin. Invest.* **113,** 1701–1710
50. De Felice, F. G., Velasco, P. T., Lambert, M. P., Viola, K., Fernandez, S. J., Ferreira, S. T., and Klein, W. L. (2007) *J. Biol. Chem.* **282,** 11590–11601
51. Zhao, W. Q., De Felice, F. G., Fernandez, S., Chen, H., Lambert, M. P., Quon, M. J., Krafft, G. A., and Klein, W. L. (2008) *FASEB J.* **22,** 246–260
52. Khosravani, H., Zhang, Y., Tsutsui, S., Hameed, S., Altier, C., Hamid, J., Chen, L., Villemaire, M., Ali, Z., Jirik, F. R., and Zamponi, G. W. (2008) *J. Cell Biol.* **181,** 551–565
53. Laurén, J., Gimbel, D. A., Nygaard, H. B., Gilbert, J. W., and Strittmatter, S. M. (2009) *Nature* **457,** 1128–1132
54. Klein, W. L., Krafft, G. A., and Finch, C. E. (2001) *Trends Neurosci.* **24,** 219–224
55. Bucciantini, M., Giannoni, E., Chiti, F., Baroni, F., Formigli, L., Zurdo, J., Taddei, N., Ramponi, G., Dobson, C. M., and Stefani, M. (2002) *Nature* **416,** 507–511
56. Walsh, D. M., Klyubin, I., Fadeeva, J. V., Cullen, W. K., Anwyl, R., Wolfe, M. S., Rowan, M. J., and Selkoe, D. J. (2002) *Nature* **416,** 535–539
57. Dickson, D. W., and Yen, S. H. (1989) *Neurobiol. Aging* **10,** 402–414
58. Terry, R. D., Masliah, E., Salmon, D. P., Butters, N., DeTeresa, R., Hill, R., Hansen, L. A., and Katzman, R. (1991) *Ann. Neurol.* **30,** 572–580
59. Thal, D. R., Rüb, U., Orantes, M., and Braak, H. (2002) *Neurology* **58,** 1791–1800
60. Hsiao, K., Chapman, P., Nilsen, S., Eckman, C., Harigaya, Y., Younkin, S., Yang, F., and Cole, G. (1996) *Science* **274,** 99–102
61. Kawarabayashi, T., Younkin, L. H., Saido, T. C., Shoji, M., Ashe, K. H., and Younkin, S. G. (2001) *J. Neurosci.* **21,** 372–381
62. Casas, C., Sergeant, N., Itier, J. M., Blanchard, V., Wirths, O., van der Kolk, N., Vingtdeux, V., van de Steeg, E., Ret, G., Canton, T., Drobecq, H., Clark, A., Bonici, B., Delacourte, A., Benavides, J., Schmitz, C., Tremp, G., Bayer, T. A., Benoit, P., and Pradier, L. (2004) *Am. J. Pathol.* **165,** 1289–1300
63. Oakley, H., Cole, S. L., Logan, S., Maus, E., Shao, P., Craft, J., Guillozet-Bongaarts, A., Ohno, M., Disterhoft, J., Van Eldik, L., Berry, R., and Vassar, R. (2006) *J. Neurosci.* **26,** 10129–10140
64. Pérez, M., Ribe, E., Rubio, A., Lim, F., Morán, M. A., Ramos, P. G., Ferrer, I., Isla, M. T., and Avila, J. (2005) *Neuroscience* **130,** 339–347
65. Wilcock, D. M., Gharkholonarehe, N., Van Nostrand, W. E., Davis, J., Vitek, M. P., and Colton, C. A. (2009) *J. Neurosci.* **29,** 7957–7965

Supplemental Material can be found at:
http://www.jbc.org/content/suppl/2008/10/10/R800036200.DC1.html
http://www.jbc.org/content/suppl/2009/02/12/284.8.4749.DC1.html

This paper is available online at www.jbc.org

THE JOURNAL OF BIOLOGICAL CHEMISTRY VOL. 284, NO. 8, pp. 4749–4753, February 20, 2009

Amyloid β-Protein Assembly and Alzheimer Disease*[S]

Published, JBC Papers in Press, October 9, 2008, DOI 10.1074/jbc.R800036200

Robin Roychaudhuri[‡], Mingfeng Yang[‡], Minako M. Hoshi[§], and David B. Teplow[‡1]

From the [‡]Department of Neurology, David Geffen School of Medicine, University of California, Los Angeles, California 90095 and the [§]Mitsubishi Kagaku Institute of Life Sciences, Tokyo 194-8511, Japan

The biochemistry of amyloid proteins has been a fascinating and important area of research because of its contribution to our understanding of protein folding dynamics and assembly and of the pathogenetic mechanisms of human disease. One such disease is AD,[2] the most common neurodegenerative disorder of aging. In AD, Aβ (Fig. 1*A*), which is expressed normally and ubiquitously throughout life as a 40–42-residue peptide, forms fibrils that deposit in the brain as "amyloid plaques." This pathologic deposition process led researchers to investigate fibril formation as a target for therapeutic intervention. In doing so, an increasing number of fibril precursors and nonfibrillar Aβ assemblies have been identified, the majority of which are neurotoxic. These findings have altered prevailing fibril-centered views of the pathobiology of amyloid diseases (1) and intensified efforts to understand the early folding and assembly dynamics of Aβ. In the discussion that follows, we seek to introduce the reader to the complex world of Aβ assembly and biological activity, a goal we hope will provide a conceptual framework upon which further knowledge or experimentation may be built.

Aβ Fibril Structure

The determination of the structure of fibrils has been an unusually difficult problem because Aβ belongs to a class of proteins that are "natively unfolded" (2) and preferentially form amyloid fibrils rather than protein crystals. This has precluded x-ray diffraction studies of full-length Aβ and made solution NMR studies problematic (3). Nevertheless, site-directed spin labeling and solid-state NMR studies have been informative. The former studies have revealed that Aβ fibrils comprise β-strands organized in a parallel, in-register fashion. The latter studies showed that in Aβ40 fibrils, residues 12–24 and 30–40 form parallel β-sheets and that these two β-strand segments are connected by a turn involving residues 25–29 (4). Hydrogen/deuterium exchange coupled with solution-state NMR revealed a similar, but distinct, segmental arrangement of β-strands within Aβ42 fibrils. Here, residues 18–26 and 31–42 form the β-strands. In both models, salt bridges between Asp^{23} and Lys^{28} stabilize the turn region connecting the two β-strands (2, 5). Similar findings have been obtained using other methods (5, 6).

Differences among the studies likely result from the examination of different peptides (Aβ40 *versus* Aβ42), the absence or presence of Met^{35}(O), or the conditions under which fibrils were formed. All these factors have been shown to affect significantly peptide assembly and biological activity (6, 7). Although no crystal structures have been determined with full-length Aβ, exciting work has been done on microcrystals formed by C-terminal peptides. These microcrystals yield diffraction patterns consistent with an in-register cross-β-organization of two interdigitated β-sheets. This "steric zipper" structure has been found in at least 13 other amyloid protein microcrystals (8). Whether steric zippers exists in Aβ fibrils is unclear.

Pathways of Peptide Assembly

How do monomers form fibrils? This question is fundamental to understanding fibrillogenesis and for identifying assembly steps that could be therapeutic targets. Influential early investigations promulgated the idea that Aβ assembly was a specific example of the general class of nucleation-dependent polymerization reactions (Fig. 1*B*). These reactions comprise a slow nucleation step, producing a "lag phase" during assembly monitoring, followed by a rapid fibril elongation step. Operating within this paradigm, nucleation (k_n) and elongation (k_e) rate constants for Aβ fibril formation were determined (9). However, continuing elucidation of this ostensibly classical polymerization process revealed unexpected complexity in the numbers and types ("on-pathway" or "off-pathway" for fibril formation) of assembly paths and the structures resulting therefrom (Fig. 1*C* and supplemental Table S1).

Protofibrils, Paranuclei, and Monomer Folds

Fig. 1*C* illustrates one pathway of fibril assembly. The penultimate fibril intermediate, the protofibril, was first identified more than a decade ago (10). Protofibrils were described as beaded chains, each bead of which was ~5 nm in diameter. The length of these structures generally was <150 nm. Kinetics and solution-phase AFM experiments showed that protofibrils matured into fibrils (10). To understand how protofibrils formed, methods were developed to determine quantitatively the oligomer size distribution in nascent Aβ preparations (11). In Aβ42 assembly, these experiments suggested that a pentamer or hexamer, the "paranucleus," was the basic unit of the protofibril and that the beaded chains comprising protofibrils formed by the self-association of paranuclei.

To understand the oligomerization process in atomic detail, computer simulations have been done (12). These studies yielded oligomer frequency distributions similar to those determined experimentally, but in addition provided high resolution

* This work was supported, in whole or in part, by National Institutes of Heath Grants NS038328 and AG027818. This work was also supported by the Jim Easton Consortium for Alzheimer's Drug Discovery and Biomarkers at UCLA and State of California Alzheimer's Disease Research Fund Grant 07-65806. This is the seventh article of eleven in the Thematic Minireview Series on the Molecular Basis of Alzheimer Disease. This minireview will be reprinted in the 2009 Minireview Compendium, which will be available in January, 2010.

[S] The on-line version of this article (available at http://www.jbc.org) contains supplemental Table S1 and additional references.

[1] To whom correspondence should be addressed. E-mail: dteplow@ucla.edu.

[2] The abbreviations used are: AD, Alzheimer disease; Aβ, amyloid β-protein; Met^{35}(O), Met^{35} sulfoxide; AFM, atomic force microscopy; CAA, cerebral amyloid angiopathy; ADDLs, Aβ-derived diffusible ligands.

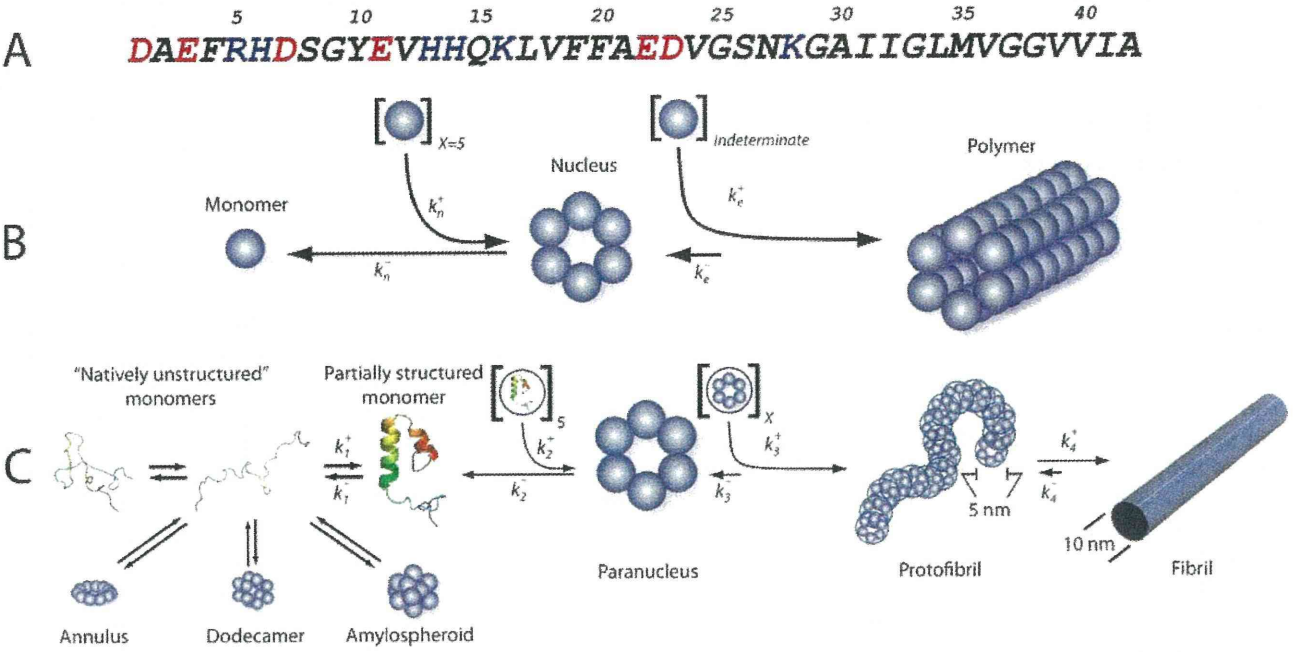

FIGURE 1. **Aβ assembly.** *A*, the sequence of Aβ42 is shown in one-letter amino acid code. The side chain charge at neutral pH is color-coded (*red*, negative; *blue*, positive). *B*, nucleation-dependent polymerization, reflecting the unfavorable self-association (rate constant $k_n^+ \ll k_n^-$) of *X* natively folded monomers (in this case, six total) to form a fibril nucleus and the favorable addition ($k_e^+ \gg k_e^-$) of a large indeterminate number of monomers to the nucleus (nascent fibril) during fibril elongation. *C*, Aβ self-assembly. Aβ belongs to the class of "natively disordered" proteins, existing in the monomer state as an equilibrium mixture of many conformers. On-pathway assembly requires the formation of a partially folded monomer that self-associates to form a nucleus for fibril elongation, a paranucleus (in this case, containing six monomers). Nucleation of monomer folding is a process distinct from fibril nucleation (50). Fibril nucleation is unfavorable kinetically ($k_2^+ \ll k_2^-$), which explains the lag phase of fibrillogenesis experiments, a period during which no fibril formation is apparent. Paranuclei self-associate readily ($k_3^+ \gg k_3^-$) to form protofibrils, which are relatively narrow (~5 nm), short (<150 nm), flexible structures. These protofibrils comprise a significant but finite number (*X*) of paranuclei. Maturation of protofibrils through a process that is kinetically favorable ($k_4^+ > k_4^-$) yields classical amyloid-type fibrils (~10-nm diameter, indeterminate (but often >1 μm) length). Other assembly pathways produce annular pore-like structures, globular dodecameric (and higher order) structures, and amylospheroids. Annuli and amylospheroids appear to be off-pathway assemblies.

conformational information. Aβ40 oligomers were more compact than Aβ42 oligomers due to increased conformational freedom of the Aβ42 N termini. This suggested that intermolecular interactions among Aβ42 N termini might facilitate the C-terminal interactions obligatory for fibril formation. The work also revealed the formation of a turn in Aβ42 at Gly^{37}-Gly^{38} that was not observed in Aβ40 and that thus could be critical in paranucleus formation.

The importance of the C terminus of Aβ in controlling Aβ assembly has also been revealed in experiments involving amino acid substitutions (11). Systematic alterations in residue 41 side chain hydrophobicity showed that Gly or Ala largely eliminated paranucleus formation, whereas amino acids with hydropathic characteristics similar to Ile had no effect. Elimination of the Ala^{42} side chain blocked paranucleus self-association, whereas insertion of larger apolar side chains facilitated the process. Similar studies examined Met^{35} polarity, an important question with respect to redox chemistry in AD (5, 11). In these experiments, oxidation of Met^{35} to Met^{35}(O) or Met^{35} sulfone had no effect on Aβ40 oligomerization, whereas Aβ42 paranucleus formation was abolished. Interestingly, the modified Aβ42 peptides oligomerized identically to Aβ40.

The relative importance of the C terminus in controlling Aβ assembly was also apparent in studies of Aβ40 and Aβ42 peptides containing substitutions linked to familial forms of AD or CAA. These substitutions ($Glu^{22} \rightarrow Gln$, $Glu^{22} \rightarrow Gly$, $Glu^{22} \rightarrow Lys$, and $Asp^{23} \rightarrow Asn$) produced oligomers of higher order when substituted in Aβ40 but had little effect on Aβ42 oligomerization. Removal of N-terminal residues Asp^1–Gly^9 in Aβ42 had no effect on its oligomer size distribution, whereas truncation of either the N-terminal two or four residues of Aβ40 produced higher-order oligomers. This observation was consistent with the aforementioned simulation data that suggested that collapse of the N terminus of Aβ40 on the oligomer surface might shield underlying hydrophobic regions of the oligomers that otherwise might interact to form higher-order assemblies (12). In fact, this process was observed in studies of the folding and assembly of urea-denatured Aβ (13). Aβ40 formed an unstable but largely collapsed monomeric species, whereas Aβ42 existed in a trimeric or tetrameric state (13).

The solvent inaccessibility of the Ala^{21}–Ala^{30} region of Aβ likely results from the formation of a turn-like structure that nucleates monomer folding (14). This decapeptide region initially was identified due to its resistance to proteolysis, a resistance that remained in the isolated decapeptide itself and that allowed NMR and computational determinations of its structure and dynamics (14). Most recently, thermodynamics studies showed that the turn is destabilized by amino acid substitutions that cause AD and CAA (15). Destabilization correlates with accelerated Aβ oligomerization and higher-order assembly and thus provides a mechanistic explanation for these familial forms of AD and CAA.

Other Assembly Pathways

The idea that an Aβ hexamer building block exists is intriguing because at least four other structures, ADDLs, Aβ*56, "globulomers," and "Aβ oligomers," comprise multiples of this basic unit (Fig. 1*C* and supplemental Table S1). ADDLs are dodecamers produced *in vitro* from Aβ42 using special solvent conditions and appear in AFM studies as globular structures with heights of 5–6 nm (16). Aβ*56 was identified in SDS extracts from brains of *Tg2576* transgenic mice (17). The "56" refers to the molecular weight of the oligomer, which is consistent with that of a dodecamer. The morphology of Aβ*56 is a prolate ellipsoid. A third type of dodecamer is the globulomer (so-called because it is a globular oligomer), which is formed by Aβ42 in the presence of SDS (18). Protease digestion, antibody binding, and mass spectrometry studies of globulomers suggest a structural model in which the hydrophobic C terminus (residues 24–42) forms a stable core and the more hydrophilic N terminus is on the surface. Although globulomers have substantial β-sheet content, presumably at the C terminus, they do not form fibrils and thus may be considered an off-pathway assembly (18). A larger species, the Aβ oligomer, also has been produced *in vitro* (19). Its molecular weight (~90,000) suggests that its assembly order is ~15–20, consistent with that of an octadecamer. In addition to assemblies with globular morphology, annular pore-like structures with diameters of 8–12 nm and pore sizes of 2–2.5 nm also have been described (10, 20).

The largest globular assemblies are amylospheroids and β-amyloid balls. Amylospheroids are off-pathway spheroidal structures with diameters of 10–15 nm that are formed by Aβ40 or Aβ42 (21). β-Amyloid balls are very large (20–200 μm) spheroidal structures formed only by Aβ40 at high concentration (300–600 μM) (22). Although such concentrations are non-physiological with respect to the average concentration of soluble Aβ *in vivo*, β-amyloid balls may be an interesting model of amyloid plaques or of the inclusion bodies formed in Parkinson and Huntington diseases and in the transmissible spongiform encephalopathies.

Assembly Complexity and Provenance

The complexity of Aβ assembly complicates the determination of precursor-product relationships. For example, are the different dodecameric assemblies discussed above really different, or are they all the same entity described in different ways by different investigators? Do the different larger spheroidal assemblies form from the same hexamer building blocks that produce dodecamers and thus belong on the same pathway? We do not know, but the answers to these questions are important because they have implications for the development of therapeutic agents targeting critical steps in the assembly pathways. For example, recent work has shown that compounds exist that can efficiently inhibit fibril formation or oligomerization, but not both (23). The distinction is critical if one assembly is benign and the other toxic.

Aβ Assembly and Disease

Thus far, we have discussed basic aspects of the physical biochemistry of Aβ assembly. However, the most fundamental biological question is, "what is the relationship between Aβ assemblies and AD?" Strong linkage exists between amyloid formation *per se* and disease (for a comprehensive review, see Ref. 24), and this linkage formed, in part, the foundation for the "amyloid cascade hypothesis," which posited that amyloid fibril formation was the key pathogenetic process in AD (25). As discussed above, elucidation of the mechanisms of fibril formation unexpectedly revealed a broad range of fibrillar and nonfibrillar structures (supplemental Table S1). Aβ oligomers appear to be particularly important because they are potent neurotoxins and are isolable from AD patients, and their concentrations correlate positively with neuropathology *in vivo*. These facts have produced a fundamental paradigm shift resulting in a revised amyloid cascade hypothesis (1, 20, 26), one that posits the primacy of oligomeric forms of Aβ in AD causation.

A substantial experimental corpus exists demonstrating that "Aβ" is neurotoxic (27). However, it was not until approximately a decade ago, with the discovery and characterization of protofibrils and ADDLs, that a more structurally precise definition of Aβ could be made, one that in turn enabled more precise structure-neurotoxicity correlations to be established (16, 28). Each new assembly subsequently discovered also was toxic. An important goal of current research is to better define the mechanisms of this toxicity, a variety of which we now discuss.

Membrane Effects

Aβ is an amphipathic peptide (Fig. 1*A*). The side chains of 16 of the first 28 residues are polar; 12 are charged at neutral pH. The remaining 12 (Aβ40) or 14 (Aβ42) side chains are apolar. Structures such as these can form micelles (29) or interact with membranes directly. Recent work has shown that Aβ40 inserts into membranes of hippocampal neurons from AD brains (30). Membrane insertion can perturb plasma membrane structure and function. For example, conformational analysis of the C-terminal domain of Aβ (residues 29–40/2) has shown it to have properties similar to those of fusion peptides of viral proteins. Insertion of these fragments in a tilted manner in the membrane is thought to disrupt the parallel symmetry of the fatty acyl chains, altering the curvature of the membrane surface and destabilizing the membrane. Consistent with this prediction, Aβ(22–42) induces membrane fusion and permeabilizes lipid vesicles that mimic neuronal membranes (31).

Aβ oligomers have also been shown to increase the conductance of lipid bilayers and living cell membranes by lowering the "dielectric barrier," possibly by increasing the membrane dielectric constant, introducing localized structural defects, or thinning the membrane (thereby facilitating charge translocation across the bilayer) (32). These effects may be related to oligomer-induced release of membrane components, including cholesterol, phospholipids, and monosialogangliosides, which in turn may lead to tau hyperphosphorylation and neurodegeneration (30, 33).

Structured membrane reorganization may also occur. Aβ40 oligomers form cation-sensitive ion channels in neuronal plasma membranes and liposomes (30, 34). These channels may comprise four to six subunits, each of which is an Aβ oligomer of order four to six, and thus the channels comprise a

total of 16–36 Aβ monomers. The channels are quasi-stable, suggesting that channel formation is a dynamic process (31). For example, Arispe *et al.* (31) have shown that Aβ40 channel activity in planar lipid bilayers results in spontaneous transitions to higher conductances. AFM images of Aβ-treated reconstituted bilayers have revealed disk-like structures with pore-like concavities of 8–12-nm outside diameter and 1–2-nm inside diameter. However, pore formation remains a contentious issue. Some believe that Aβ oligomer-mediated interference with the surface packing of lipid headgroups effectively thins the membrane, reduces effective membrane conductance, and may produce the appearance of pores. Time-lapse AFM experiments have revealed that Aβ aggregates ~500 nm in size form along the edges of bilayer defects, a result that could be misinterpreted as pore formation (35). Consistent with this interpretation are recent results suggesting that oligomers alter membrane conductivity without forming discrete pores (32).

We note that two general classes of Aβ/membrane interaction may occur: 1) nonreceptor-mediated structural interactions of the type discussed above; and 2) specific receptor-mediated interactions. These latter interactions may involve fibrillar and oligomeric forms of Aβ that act either as agonists or antagonists. Many membrane Aβ receptors have been identified (30), but the important question that remains unanswered is whether these interactions are physiologically relevant or serendipitous.

Metals, Aggregation, and Radicals

Evidence exists that metals are involved in the pathogenesis of AD. However, this is a contentious issue that remains unresolved. We present here a number of prominent mechanistic hypotheses.

In vitro results indicate that physiological concentrations of Zn^{2+} and Cu^{2+} can accelerate Aβ aggregation and increase Aβ toxicity (36, 37). Aβ has a strong positive reduction potential and displays high-affinity binding for Cu^{2+}, Zn^{2+}, and Fe^{3+} ions (34). Solution-state NMR and EPR have suggested that the three His residues in Aβ, His^6, His^{13}, and His^{14}, coordinate Cu^{2+}. This metalloenzyme-like complex has been proposed to catalyze Fenton chemistry (Equation 1),

$$Me^{n+} + H_2O_2 \rightarrow Me^{(n+1)+} + OH^{\bullet} + OH^{-} \quad \text{(Eq. 1)}$$

which yields toxic hydroxyl ($OH^{\bullet}$) and peroxide ($OOH^{\bullet}$) radicals. Fe^{2+} is also thought to participate in this chemistry. In addition to its postulated catalytic role in Fenton chemistry, it has been suggested that Aβ-linked inhibition of catalase increases H_2O_2 production (Equation 2) (38).

$$Me^{(n+1)+} + H_2O_2 \rightarrow Me^{n+} + OOH^{\bullet} + H^{+} \quad \text{(Eq. 2)}$$

A second center for redox chemistry is Met^{35} (39). The generation of reactive oxygen species by Aβ requires reduction of Cu^{2+} or Fe^{3+}, a reaction that may proceed through the oxidation of Met^{35} to its corresponding sulfide radical cation. Cu^{+} or Fe^{2+} produced in this way may react with molecular oxygen and biological reducing agents (*e.g.*; cholesterol, vitamin C, or catecholamine) to yield H_2O_2 and the starting Cu^{+} cation (40). The H_2O_2 thus produced can further oxidize Met^{35} to its sulfoxide form and also react with superoxide anion (O_2^{-}) in a Haber-Weiss reaction to produce $OH^{\bullet}$ (Equation 3).

$$O_2^{-} + H_2O_2 \rightarrow OH^{\bullet} + OH^{-} + O_2 \quad \text{(Eq. 3)}$$

Interestingly, the $Met^{35}(O)$ and Met^{35} sulfone forms of Aβ do not assemble as does the wild-type peptide (11, 41). Hou *et al.* (41) have reported that oxidation of Met^{35} to $Met^{35}(O)$ significantly reduces the rate of amyloid formation and alters fibril morphology. Bitan and Teplow (11) reported similar findings and found that $Met^{35}(O)$ Aβ42 does not form paranuclei, but rather oligomerizes similarly to Aβ40. These *in vitro* observations are consistent with the strong negative correlation that exists between oxidative damage and Aβ deposition in AD (11, 39).

Murakami *et al.* (42) have proposed that Tyr^{10} is also involved in redox chemistry. They suggested that H_2O_2 produced by Aβ-metal complexes oxidizes Tyr^{10} to produce the tyrosyl radical, which then attacks the thioether of Met^{35} and yields an *S*-oxidized radical cation. A turn at Gly^{38}–Val^{39} brings the C-terminal carboxylate anion proximate to the radical, stabilizing it and simultaneously creating a hydrophobic subdomain facilitating peptide oligomerization, fibril formation, and longer lasting oxidative stress.

Mitochondrial Effects

Mitochondrial dysfunction has been linked directly to the aging process (43), a process that is the largest single risk factor for AD. Exacerbation of age-related dysfunction by toxic Aβ assemblies may explain the linkage of both age and Aβ to AD. Increasing evidence suggests that Aβ-induced mitochondrial dysfunction does in fact occur. The interaction of full-length Aβ or truncated forms with mitochondria causes potent inhibition of electron transport chain enzyme complexes and reductions in the activities of tricarboxylic acid cycle enzymes, leading to inhibition of ATP production, mitochondrial swelling, cytochrome *c* release, caspase activation, transition pore opening, increased mitochondrial reactive oxygen species production, and decreased mitochondrial membrane potential and respiration rates (43, 44). Complexation of Aβ with Aβ-binding alcohol dehydrogenase, a mitochondrial matrix enzyme, or with endoplasmic reticulum-associated Aβ-binding protein also produces this type of damage (45).

Apoptosis

A common final pathway of Aβ-induced neuronal dysfunction is apoptosis. This pathway is particularly likely to occur following mitochondrial compromise. Aβ40 and Aβ42 oligomers also have been shown recently to activate sphingomyelinases, which results in apoptotic cell death through a redox-sensitive cytosolic phospholipase A_2/arachidonic acid-dependent pathway (46). In rat hippocampal neuron cultures, activation of ERK1/2 (extracellular signal-regulated kinase-1/2) by Aβ oligomers results in caspase-3 activation, tau cleavage, dysregulation of cell structure, and finally apoptosis (47). Transforming growth factor-β1 has been found to exacerbate Aβ-induced toxicity through Smad7 and β-catenin interac-

tions and nuclear localization. Aβ40 also can activate the NF-κB apoptosis pathway by selectively inducing the nuclear translocation of the NF-κB p65 and p50 subunits. For this reason, p65 and p50 have been suggested as AD therapeutic targets. The connection of apoptosis with Aβ assemblies is supported by the observation that up-regulation in neurons of peroxisome proliferator-activated receptor-γ, which increases expression of the anti-apoptotic protein Bcl-2, protects these cells against Aβ-induced toxicity (48).

An Explication

The impetus for studies of Aβ structure, dynamics, and bioactivity has been the causal link of Aβ to AD. The result of these studies has been an extraordinary expansion of knowledge. The rapidly increasing number of clinical trials of mechanistically novel AD therapies suggests that this knowledge has been of value (49). However, a consensus does not exist regarding either the biophysical or biological behavior of Aβ. For academics, rigorous experiments done in well controlled systems provide reliable, although not necessarily clinically relevant, information. However, for AD patients, their families, and the treating clinicians, relevance is paramount. For their sake, it is hoped that the information presented here will stimulate current and especially new researchers to conceive of novel experimental approaches seeking to answer three fundamental questions. 1) Is Aβ, in fact, the proximate etiologic agent of AD; 2) if so, what is the structure of the proximate neurotoxic Aβ assembly; and 3) if not, what is?

REFERENCES

1. Kirkitadze, M. D., Bitan, G., and Teplow, D. B. (2002) *J. Neurosci. Res.* **69,** 567–577
2. Nelson, R., and Eisenberg, D. (2006) *Curr. Opin. Struct. Biol.* **16,** 260–265
3. Teplow, D. B. (2006) *Methods Enzymol.* **413,** 20–33
4. Tycko, R. (2006) *Methods Enzymol.* **413,** 103–122
5. Finder, V. H., and Glockshuber, R. (2007) *Neurodegener. Dis.* **4,** 13–27
6. Fändrich, M. (2007) *CMLS Cell. Mol. Life Sci.* **64,** 2066–2078
7. Kodali, R., and Wetzel, R. (2007) *Curr. Opin. Struct. Biol.* **17,** 48–57
8. Sawaya, M. R., Sambashivan, S., Nelson, R., Ivanova, M. I., Sievers, S. A., Apostol, M. I., Thompson, M. J., Balbirnie, M., Wiltzius, J. J. W., McFarlane, H. T., Madsen, A., Riekel, C., and Eisenberg, D. (2007) *Nature* **447,** 453–457
9. Teplow, D. B. (1998) *Amyloid* **5,** 121–142
10. Caughey, B., and Lansbury, P. T. (2003) *Annu. Rev. Neurosci.* **26,** 267–298
11. Bitan, G., and Teplow, D. B. (2004) *Acc. Chem. Res.* **37,** 357–364
12. Urbanc, B., Cruz, L., Yun, S., Buldyrev, S. V., Bitan, G., Teplow, D. B., and Stanley, H. E. (2004) *Proc. Natl. Acad. Sci. U. S. A.* **101,** 17345–17350
13. Chen, Y.-R., and Glabe, C. G. (2006) *J. Biol. Chem.* **281,** 24414–24422
14. Teplow, D. B., Lazo, N. D., Bitan, G., Bernstein, S., Wyttenbach, T., Bowers, M. T., Baumketner, A., Shea, J.-E., Urbanc, B., Cruz, L., Borreguero, J., and Stanley, H. E. (2006) *Acc. Chem. Res.* **39,** 635–645
15. Grant, M. A., Lazo, N. D., Lomakin, A., Condron, M. M., Arai, H., Yamin, G., Rigby, A. C., and Teplow, D. B. (2007) *Proc. Natl. Acad. Sci. U. S. A.* **104,** 16522–16527
16. Lambert, M. P., Barlow, A. K., Chromy, B. A., Edwards, C., Freed, R., Liosatos, M., Morgan, T. E., Rozovsky, I., Trommer, B., Viola, K. L., Wals, P., Zhang, C., Finch, C. E., Krafft, G. A., and Klein, W. L. (1998) *Proc. Natl. Acad. Sci. U. S. A.* **95,** 6448–6453
17. Lesné, S., Koh, M. T., Kotilinek, L., Kayed, R., Glabe, C. G., Yang, A., Gallagher, M., and Ashe, K. H. (2006) *Nature* **440,** 352–357
18. Gellermann, G. P., Byrnes, H., Striebinger, A., Ullrich, K., Mueller, R., Hillen, H., and Barghorn, S. (2008) *Neurobiol. Dis.* **30,** 212–220
19. Deshpande, A., Mina, E., Glabe, C., and Busciglio, J. (2006) *J. Neurosci.* **26,** 6011–6018
20. Haass, C., and Selkoe, D. J. (2007) *Nat. Rev. Mol. Cell Biol.* **8,** 101–112
21. Hoshi, M., Sato, M., Matsumoto, S., Noguchi, A., Yasutake, K., Yoshida, N., and Sato, K. (2003) *Proc. Natl. Acad. Sci. U. S. A.* **100,** 6370–6375
22. Westlind-Danielsson, A., and Arnerup, G. (2001) *Biochemistry* **40,** 14736–14743
23. Necula, M., Kayed, R., Milton, S., and Glabe, C. G. (2007) *J. Biol. Chem.* **282,** 10311–10324
24. Sipe, J. C. (ed) (2005) *Amyloid Proteins: The Beta Sheet Conformation and Disease*, Wiley-VCH, Weinheim, Germany
25. Hardy, J. (1996) *Ann. Med.* **28,** 255–258
26. Hardy, J., and Selkoe, D. J. (2002) *Science* **297,** 353–356
27. Yankner, B. A., and Lu, T. (2009) *J. Biol. Chem.* **284,** 4755–4759
28. Walsh, D. M., Hartley, D. M., Kusumoto, Y., Fezoui, Y., Condron, M. M., Lomakin, A., Benedek, G. B., Selkoe, D. J., and Teplow, D. B. (1999) *J. Biol. Chem.* **274,** 25945–25952
29. Lomakin, A., Chung, D. S., Benedek, G. B., Kirschner, D. A., and Teplow, D. B. (1996) *Proc. Natl. Acad. Sci. U. S. A.* **93,** 1125–1129
30. Verdier, Y., Zarndi, M., and Penke, B. (2004) *J. Pept. Sci.* **10,** 229–248
31. Arispe, N., Diaz, J. C., and Simakova, O. (2007) *Biochim. Biophys. Acta* **1768,** 1952–1965
32. Sokolov, Y., Kozak, J. A., Kayed, R., Chanturiya, A., Glabe, C., and Hall, J. E. (2006) *J. Gen. Physiol.* **128,** 637–647
33. Tashima, Y., Oe, R., Lee, S., Sugihara, G., Chambers, E. J., Takahashi, M., and Yamada, T. (2004) *J. Biol. Chem.* **279,** 17587–17595
34. Kawahara, M., Arispe, N., Kuroda, Y., and Rojas, E. (1997) *Biophys. J.* **73,** 67–75
35. Green, J. D., Kreplak, L., Goldsbury, C., Blatter, X. L., Stolz, M., Cooper, G. S., Seelig, A., Kistler, J., and Aebi, U. (2004) *J. Mol. Biol.* **342,** 877–887
36. Jun, S., and Saxena, S. (2007) *Angew. Chem. Int. Ed. Engl.* **46,** 5251–5263
37. Bush, A. I. (2003) *Trends Neurosci.* **26,** 207–214
38. Behl, C., Davis, J. B., Lesley, R., and Schubert, D. (1994) *Cell* **77,** 817–827
39. Butterfield, D. A. (2003) *Curr. Med. Chem.* **10,** 2651–2659
40. Crouch, P. J., Harding, S.-M. E., White, A. R., Camakaris, J., Bush, A. I., and Masters, C. L. (2008) *Int. J. Biochem. Cell Biol.* **40,** 181–198
41. Hou, L., Kang, I., Marchant, R. E., and Zagorski, M. G. (2002) *J. Biol. Chem.* **277,** 40173–40176
42. Murakami, K., Irie, K., Ohigashi, H., Hara, H., Nagao, M., Shimizu, T., and Shirasawa, T. (2005) *J. Am. Chem. Soc.* **127,** 15168–15174
43. Crouch, P. J., Cimdins, K., Duce, J. A., Bush, A. I., and Trounce, I. A. (2007) *Rejuvenation Res.* **10,** 349–357
44. Mancuso, C., Scapagini, G., Curr, D., Stella, A. M. G., Marco, C. D., Butterfield, D. A., and Calabrese, V. (2007) *Front. Biosci.* **12,** 1107–1123
45. Chen, J. X., and Yan, S. D. (2007) *J. Alzheimer's Dis.* **12,** 177–184
46. Malaplate-Armand, C., Florent-Bchard, S., Youssef, I., Koziel, V., Sponne, I., Kriem, B., Leininger-Muller, B., Olivier, J.-L., Oster, T., and Pillot, T. (2006) *Neurobiol. Dis.* **23,** 178–189
47. Chong, Y. H., Shin, Y. J., Lee, E. O., Kayed, R., Glabe, C. G., and Tenner, A. J. (2006) *J. Biol. Chem.* **281,** 20315–20325
48. Fuenzalida, K., Quintanilla, R., Ramos, P., Piderit, D., Fuentealba, R. A., Martinez, G., Inestrosa, N. C., and Bronfman, M. (2007) *J. Biol. Chem.* **282,** 37006–37015
49. Yamin, G., Ono, K., Inayathullah, M., and Teplow, D. B. (2008) *Curr. Pharm. Des.* **14,** 3231–3246
50. Lazo, N. D., Grant, M. A., Condron, M. C., Rigby, A. C., and Teplow, D. B. (2005) *Protein Sci.* **14,** 1581–1596

Chemical Science

View Online
Dynamic Article Links

Cite this: DOI: 10.1039/c1sc00071c

www.rsc.org/chemicalscience

EDGE ARTICLE

^{19}F MRI detection of β-galactosidase activity for imaging of gene expression†

Shin Mizukami,[ab] Hisashi Matsushita,[a] Rika Takikawa,[a] Fuminori Sugihara,[c] Masahiro Shirakawa[d] and Kazuya Kikuchi*[ab]

Received 3rd February 2011, Accepted 23rd March 2011
DOI: 10.1039/c1sc00071c

Imaging of gene expression by magnetic resonance imaging (MRI) yields direct information regarding living systems that cannot be obtained *via* other methods. In this study, we report the rational design and synthesis of a novel ^{19}F MRI probe that detects β-galactosidase (β-gal) activity, enabling the imaging of gene expression in cells. The ^{19}F MRI signal of the probe was quenched by the intramolecular paramagnetic resonance enhancement from a Gd^{3+} ion. A contrivance was made in the probe structure to recover the ^{19}F MRI signal after hydrolysis by β-gal with a following self-immolative reaction. This ^{19}F MRI signal change was observed in the physiological aqueous condition. The probe could also detect β-gal activity in fixed HEK293T cells. In conclusion, this new probe enables the ^{19}F MRI detection of cellular gene expression. The probe design strategy is also expected to lead to the development of MRI probes for a wide variety of hydrolase activities.

Introduction

Imaging of gene expression gives us various information such as the expression timing of target proteins, gene transfer efficiency, and detection of a disease-related gene expression. To monitor gene expression by various methods, reporter proteins[1–3] are useful. Fluorescence detection of gene expression by using fluorescent proteins is particularly important because fluorescence measurement has several advantages including sensitivity, convenience, spatiotemporal resolution, *etc.* However, the poor transmission of fluorescence is one of the limitations for the *in vivo* application. Use of magnetic resonance imaging (MRI)[4] is one way to solve the problem, because MRI yields high-resolution images of deep regions of living animal bodies. Therefore, MRI is currently considered to be one of the most promising techniques for *in vivo* investigation of physiological events.[5]

Recently, several smart ^{1}H MRI probes for visualizing gene expression *via* β-galactosidase activity have been reported.[6] In principle, however, such ^{1}H MRI signal enhancement needs to be discriminated from the background ^{1}H MRI signals of water, fatty acids, and other biomolecules. To avoid this limitation, we have focused on the use of ^{19}F MRI. ^{19}F, as well as ^{1}H, is one of the most highly sensitive nuclei for NMR spectroscopy and MRI,[7] and almost no intrinsic ^{19}F MRI signals are observed in animal bodies. Thus, ^{19}F MRI probes that can visualize biological events have been increasingly reported.[8] We have also developed off-on switching ^{19}F MRI probes to detect protease activity[9] on the basis of paramagnetic relaxation enhancement (PRE),[10] a phenomenon in which the relaxation of nuclei is enhanced near paramagnetic molecules.

By expanding this probe principle, we here report a novel ^{19}F MRI probe that detects cellular gene expression. β-galactosidase (β-gal) was chosen as the reporter protein for gene expression, because it has several advantages where reporter proteins are concerned.[3,11] The advantages are as follows: (1) induction of β-gal synthesis occurs over a large dynamic range, (2) β-gal is tolerated and functional in many organisms including mammals, (3) various substrates of β-gal are available or easily synthesized, (4) many assay methods that use β-D-galactopyranoside-coupled aglycones are available, and (5) there is almost no intrinsic β-gal activity in mammalian cells. Therefore, β-gal is one of the most widely used reporter proteins for imaging of gene expression. Through the detection of β-gal activity, we tried ^{19}F MRI detection of cellular gene expression.

Results

Probe design concept, synthesis and physical properties

Several probes have been developed that can detect β-gal activity.[3,12] X-gal is one of the most widely used probes among them. Such β-D-galactopyranoside-coupled aromatic compounds are known to be the substrates of β-gal, and several fluorescent probes for β-gal have been developed. Taking this substrate

[a]*Division of Advanced Science and Biotechnology, Graduate School of Engineering, Osaka University, 2-1 Yamadaoka, Suita, Osaka, 565-0871, Japan. E-mail: kkikuchi@mls.eng.osaka-u.ac.jp; Fax: (+81) 6-6879-7875*
[b]*Immunology Frontier Research Center (IFReC), Osaka University, Osaka, 565-0871, Japan*
[c]*International Graduate School of Arts and Sciences, Yokohama City University, Kanagawa, 230-0045, Japan*
[d]*Graduate School of Engineering, Kyoto University, Kyoto, 615-8510, Japan*

† Electronic supplementary information (ESI) available: Synthesis of compounds, representative HPLC chromatograms and ^{19}F NMR. See DOI: 10.1039/c1sc00071c

recognition property of β-gal into consideration, we designed a ^{19}F MRI probe Gd-DFP-Gal for detecting β-gal activity by combining the paramagnetic relaxation enhancement (PRE) based probe design principle that we previously developed[9] with the structures of conventional β-gal probes (Fig. 1). The transverse relaxation time T_2 of the ^{19}F nucleus near Gd^{3+} is expected to be reduced by the PRE from Gd^{3+}, which has seven unpaired electrons in its 4f orbital. Thus, the T_2 of the trifluoromethyl (CF_3) group of Gd-DFP-Gal was expected to be strongly reduced.

Another designed function of Gd-DFP-Gal is the self-immolative property that can be induced by enzymatic cleavage. When Gd-DFP-Gal is hydrolyzed by β-gal, the probe is expected to be automatically converted to the corresponding quinone methide by the successive elimination of the substituent at the benzyl position.[13] Thus, the T_2 of the trifluoromethyl group extends after the β-galactoside bond is cleaved because of the cancellation of the intramolecular PRE. MRI signal intensity (*i.e.*, the peak height of the NMR signal) is proportional to $\exp(-t/T_2)$, where t is the echo time in the spin-echo method. Thus, the T_2 extension leads to an increase in the MRI signal. On the basis of this principle, we expected that the originally quenched ^{19}F MRI signal of Gd-DFP-Gal would emerge upon the enzyme reaction.

Gd-DFP-Gal was synthesized in five steps (Scheme S1, ESI†). Details of the synthetic procedure are described in the Supporting Information.† As we expected, the NMR peak of Gd-DFP-Gal was not observed, although that of the Gd-free probe DFP-Gal was a sharp single peak (Fig. S2, ESI†). Disappearance of the ^{19}F NMR peak of Gd-DFP-Gal indicates that the T_2 was markedly reduced because of the strong intramolecular PRE.

In vitro detection of β-gal activity by ^{19}F NMR and ^{19}F MRI

Because the relaxation times of Gd-DFP-Gal were dramatically reduced, it was expected that the enzymatic degradation of Gd-DFP-Gal would induce the recovery of the disappeared ^{19}F NMR peak. Gd-DFP-Gal was incubated with β-gal at 37 °C in the reaction buffer (pH 7.3) containing 5% D_2O, and the time course of the ^{19}F NMR peak was monitored (Fig. 2a). A single peak appeared at around 16 ppm (internal standard: sodium trifluoroacetate) and increased in a time-dependent manner. As the progress of the enzyme reaction was confirmed by RP-HPLC, the peak of Gd-DFP-Gal disappeared and a new peak appeared (Fig. 2b). The new peak was identified to be 4-hydroxymethyl-3-trifluoromethylphenol (compound **2**) from the retention time. In addition, the ESI-MS of the HPLC peak fraction gave a molecular weight identical to **2** ($m/z = 192$). No other noticeable peaks in the reaction solution HPLC diagram suggest that Gd-DFP-Gal was converted to **2** by β-galactosidase activity with nearly complete efficiency.

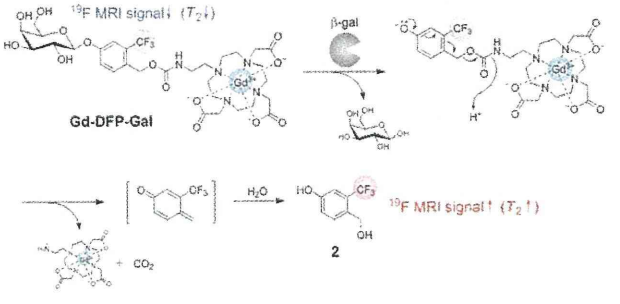

Fig. 1 Structure of Gd-DFP-Gal and the principle for the ^{19}F MRI detection of β-gal activity.

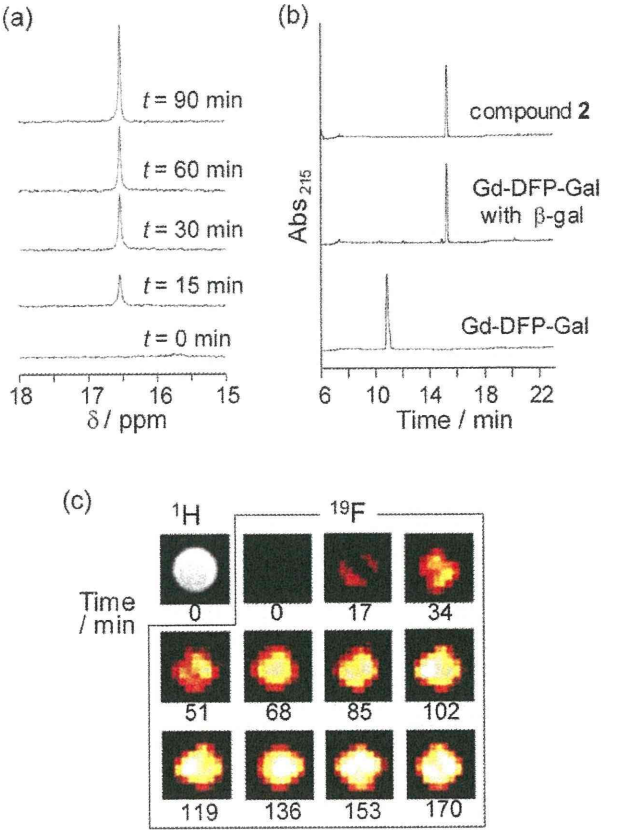

Fig. 2 Detection of β-gal activity by Gd-DFP-Gal. (a) Time-dependent ^{19}F NMR spectral change of Gd-DFP-Gal (1 mM) under incubation with β-gal. Sodium trifluoroacetate was used as the internal standard (0 ppm). (b) Confirmation of the enzymatic cleavage by RP-HPLC (eluent: H_2O–acetonitrile containing 0.1% TFA). (c) Time course of the density-weighted ^{19}F MR phantom images of Gd-DFP-Gal (1 mM) at 37 °C after β-gal was added.

The relaxation times T_1 and T_2 of the reaction sample became 0.306 s and 0.086 s, respectively, after the enzyme reaction. Both of them showed considerable extension compared to those of Gd-DFP-Gal, probably due to the cancellation of the intramolecular PRE from Gd^{3+}. These values are still less than those of the Gd^{3+}-free probe DFP-Gal: 1.293 s for T_1 and 0.271 s for T_2. When the relaxation times of Gd-DFP-Gal were measured at various probe concentrations after the enzymatic cleavage, both T_1 and T_2 extended as the concentration decreased (Fig. S3 and Table S1, ESI†). This concentration dependency of the relaxation times indicates that the intermolecular PRE is effective under the experimental condition even after the enzyme reaction is complete. To confirm the probe specificity, Gd-DFP-gal was incubated with other similar enzymes, α-galactosidase and β-glucuronidase. However, ^{19}F NMR signals of Gd-DFP-gal were not recovered by incubation with such enzymes (Fig. S4, ESI†).

To demonstrate the possibility of further application, ^{19}F MRI detection of β-gal activity was performed using Gd-DFP-Gal. ^{19}F MRI phantom images were measured using an 11.7 T MRI instrument. Gd-DFP-Gal was mixed with *Escherichia coli* β-gal before being poured into a 1-mm-inner radius capillary. The density-weighted MR images were then captured by the fast spin-echo method. As expected from the ^{19}F NMR results, Gd-DFP-Gal showed no ^{19}F MRI signals in the absence of β-gal. After the probe was mixed with β-gal, however, the ^{19}F MRI signals gradually increased in a time-dependent manner (Fig. 2c). Without addition of the enzyme, the MRI image did not show any signals for several hours (data not shown). These results demonstrate that this novel mechanism-based probe Gd-DFP-Gal enables the specific ^{19}F MRI detection of β-gal activity.

^{19}F NMR and ^{19}F MRI detection of β-gal expression in fixed HEK293T cells

Next, the applicability of Gd-DFP-Gal to the detection of intracellular gene expression was confirmed. β-gal was expressed in HEK293T cells, and the cells were fixed with formaldehyde and detergent. Then, Gd-DFP-Gal was incubated with the cells, and β-gal activity in the medium supernatant was analyzed by ^{19}F NMR (Fig. 3a). As a result, incubation of Gd-DFP-Gal only with the cells expressing β-gal induced the clear increase of a single ^{19}F NMR peak (Fig. 3b).

Then, the ^{19}F MRI detection of β-gal gene expression was attempted. HEK293T cells expressing or not expressing β-gal were cultured on 7-mm-diameter glass vessels. After the fixation of the cells, Gd-DFP-Gal (final conc.: 1 mM) was added into the glass vessels, and the cells were incubated at 37 °C for 2 h. The vessels were stacked in an 8 mm NMR tube, as shown in Fig. 3b, and the ^{1}H and ^{19}F MR images were captured. Although both vessels showed indistinguishable signal intensity in ^{1}H MRI (Fig.3c left), only the vessel that included HEK293T cells expressing β-gal showed remarkable ^{19}F MRI signals (Fig. 3c right). These results indicate that Gd-DFP-Gal can specifically detect gene expression in fixed HEK293T cells by means of reporter β-gal activity.

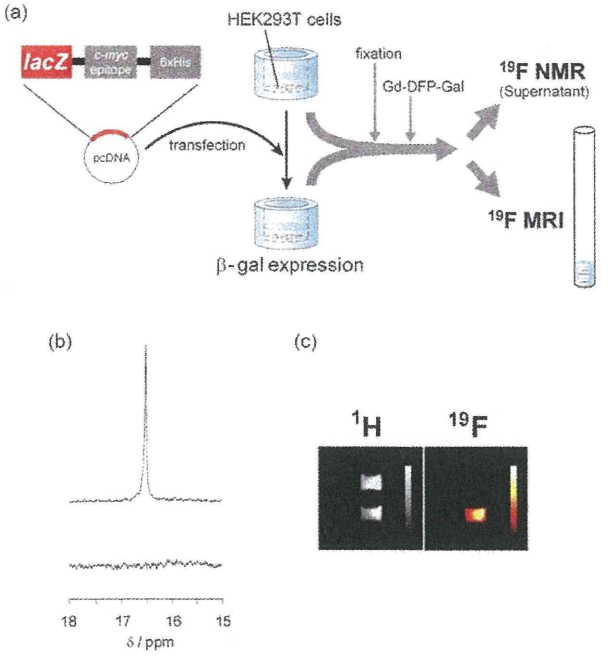

Fig. 3 ^{19}F NMR and ^{19}F MRI detection of gene expression in HEK293T cells. (a) Illustration of the experimental procedures for the ^{19}F NMR and ^{19}F MRI measurements. (b) ^{19}F NMR spectra of the culture medium containing 1 mM Gd-DFP-Gal incubated with fixed cells expressing (top) or not expressing (bottom) β-gal. (c) ^{1}H (left) and ^{19}F (right) MR images of culture vessels containing 1 mM Gd-DFP-Gal fixed cells. Color scale bars were inserted in the images.

Discussion

From the point of probe design strategy, development of Gd-DFP-Gal is an important step forward in molecular imaging studies. Our previous ^{19}F MRI probe that detects protease activity also utilized the cancellation of the intramolecular PRE for signal switching.[9] In these cases, the ^{19}F atoms and the paramagnetic ions were conjugated to each other at the opposite end of the probes (Fig. 4a). The MRI signals were enhanced by enzymatic cleavage of the substrate linker. Although this strategy works for a wide variety of hydrolases such as other proteases, endonucleases and phosphodiesterases, it could not be applied to several hydrolases such as phosphatases that have a substrate-binding pocket covering one end of the substrate. In order to detect these enzyme activities by MRI, we expanded the probe design concept by exploiting a self-immolative reaction, as presented in this study (Fig. 1). We now have the ability to design ^{19}F MRI probes for a broader range of hydrolases by choosing either of the ways illustrated in Fig. 4.

Although imaging of gene expression in fixed cells by using Gd-DFP-Gal, there are two obstacles for future perspective to *in vivo* imaging. One is the membrane permeability of the probes. Since the new probe did not permeate cell membrane, the cells needed to be fixed with formaldehyde for imaging. However, use of cell-penetrating peptides,[14] which enabled the incorporation of proteins into live cells, may dissolve the problem.

The other is the sensitivity. Generally, the sensitivity of ^{19}F MRI probes is worse than ^{1}H MRI probes. This is because ^{1}H MRI visualizes many water molecules around the probe

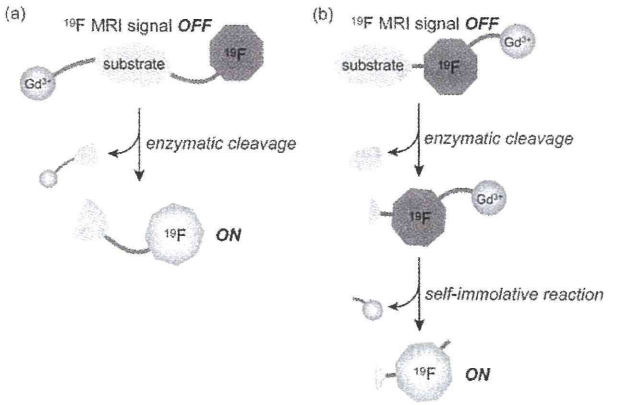

Fig. 4 Two ^{19}F MRI probe design strategies using PRE cancellation by (a) enzymatic cleavage of the substrate linker, and (b) enzyme activity-induced self-immolative reaction.

molecules, although ^{19}F MRI probes give only the probe signals. Concerning the problem, improvement of both probes and instruments will contribute to solve it. About the probe sensitization, we are under the development and would report elsewhere in future.

Conclusions

In summary, we succeeded in the imaging of gene expression in mammalian cells using a novel ^{19}F MRI probe that detects β-gal activity. The probe design concept is based on the MRI signal quenching by PRE. Also, by exploiting a self-immolative organic reaction in the probe design, we could overcome the limitation of our previous probe design, in which the ^{19}F atoms and the paramagnetic ions should be located at the opposite end of the probes. New design strategy will lead to the development of the probes for a wider variety of hydrolases such as phosphatases. Although *in vivo* imaging of gene expression by ^{19}F MRI is still challenging, the further progress of the probe properties will contribute to the solution of the difficult and significant subject.

Experimental section

^{19}F NMR relaxation time measurements

Samples were prepared at 500 μM concentration in 10 mM Tris buffer (pH 7.3) containing 10 mM magnesium chloride and 5% D_2O. The longitudinal relaxation time T_1 was measured by an inversion recovery method and the transverse relaxation time T_2 was measured by the spin-echo method.

Enzyme reaction

Gd-DFP-Gal was dissolved at 500 μM in 10 mM Tris buffer (pH 7.3) containing 10 mM magnesium chloride and 5% D_2O. Samples (500 μL) were incubated with β-gal (5.03 U) at 37 °C for 2 h. The reaction progress was monitored by ^{19}F NMR and RP-HPLC using an octadecyl silane (ODS) column. For the ^{19}F MRI experiment, 1 mM Gd-DFP-Gal was dissolved in 10 mM Tris buffer solution (pH 7.3) containing 10 mM magnesium chloride and 5% D_2O. Samples with or without β-gal (1.2 mU) were filled into glass capillaries (inner diameter: approximately 1 mm; Hischmann Laborgerate). The capillaries were then inserted into an 8 mm NMR tube and the ^{19}F MRI were measured.

Cellular experiments

HEK293T cells were grown at 37 °C in Dulbecco's modified Eagle's medium (DMEM) supplemented with 10% fetal bovine serum (FBS), 100 U mL^{-1} penicillin G, and 100 mg mL^{-1} streptomycin in a humidified atmosphere with 5% CO_2. The cells were plated at 1.2×10^6 cells in 60 mm dishes or 1.2×10^5 cells cm^{-2} on 24-well plates. Next, the cells were transfected with pcDNA™4/TO/*myc*-His/*lacZ*© plasmid using Lipofectamine 2000, and the cells were incubated for 24 h at 37 °C in a CO_2 incubator. After the cells were washed three times with phosphate-buffered solution (PBS), they were incubated with trypsin-EDTA at 37 °C for 5 min under 5% CO_2.

For ^{19}F NMR analysis, the cells were cultured with 1 mM Gd-DFP-Gal for 2 h at 37 °C in the reaction buffer (10 mM Tris-sodium buffer (pH 7.3) and 10 mM magnesium chloride) on 24-well plates. Then, the supernatants were moved into NMR tubes and the ^{19}F NMR spectra were measured.

For ^{19}F MRI analysis, the cells were moved onto 7 mm (outer diameter) glass vessels (Hilgenberg GmbH), and were incubated for 7 h at 37 °C in DMEM with 10% FBS. After the cells were washed three times with PBS, they were incubated with 3.7% formaldehyde for 10 min at room temperature. Then, cells were washed three times with PBS and incubated with 1 mM Gd-DFP-Gal for 2 h at 37 °C in the reaction buffer (Tris-sodium buffer (pH 7.3) and 10 mM magnesium chloride). The vessels were put into an 8 mm NMR tube, and the ^1H and ^{19}F MRI were measured.

Acknowledgements

We thank Dr Tetsuro Kokubo at Yokohama City University for the use of the MRI instrument, and Dr Haruhiko Bito (University of Tokyo), Dr Hiroyuki Okuno (University of Tokyo) and Dr Shin-ichi Muramatsu (Jichi Medical University) for the helpful discussion. This research is supported by Ministry of Education, Culture, Sports, Science and Technology–Japan (Grant No. 21685019 and 20675004), by the Japan Society for the Promotion of Science (JSPS) through its Funding Program for World-Leading Innovative R&D on Science and Technology (FIRST Program), by Ministry of Health, Labour and Welfare–Japan, and by the New Energy and Industrial Technology Development Organization (NEDO) of Japan. S.M. acknowledges the Inamori Foundation.

Notes and references

1 R. Y. Tsien, *Annu. Rev. Biochem.*, 1998, **67**, 509.
2 C. H. Contag and M. H. Bachman, *Annu. Rev. Biomed. Eng.*, 2002, **4**, 235.
3 (*a*) G. P. Nolan, S. Fiering, J.-F. Nicholas and L. A. Herzenberg, *Proc. Natl. Acad. Sci. U. S. A.*, 1988, **85**, 2603; (*b*) I. G. Serebriiskii and E. A. Golemis, *Anal. Biochem.*, 2000, **285**, 1.
4 (*a*) A. Jasanoff, *Trends Neurosci.*, 2005, **28**, 120; (*b*) D. E. Sosnovik and R. Weissleder, *Curr. Opin. Biotechnol.*, 2007, **18**, 4.
5 (*a*) R. Weissleder and M. J. Pittet, *Nature*, 2008, **452**, 580; (*b*) J. L. Major and T. J. Meade, *Acc. Chem. Res.*, 2009, **42**, 893.
6 (*a*) A. Y. Louie, M. M. Hüber, E. T. Ahrens, U. Rothbächer, R. Moats, R. E. Jacobs, S. E. Fraser and T. J. Meade, *Nat. Biotechnol.*, 2000, **18**, 321; (*b*) Y. T. Chang, C. M. Cheng, Y. Z. Su, W. T. Lee, J. S. Hsu, G. C. Liu, T. L. Cheng and Y. M. Wang, *Bioconjugate Chem.*, 2007, **18**, 1716; (*c*) E. L. Que, D. W. Domaille and C. J. Chang, *Chem. Rev.*, 2008, **108**, 1517; (*d*) W. Cui, L. Liu, V. D. Kodibagkar and R. P. Mason, *Magnetic Resonance in Medicine*, 2010, **64**, 65.
7 (*a*) J. Yu, V. D. Kodibagkar, W. Cui and R. P. Mason, *Curr. Med. Chem.*, 2005, **12**, 819; (*b*) C. Belle, C. Beguin, S. Hamman and J.-L. Pierre, *Coord. Chem. Rev.*, 2009, **253**, 963.
8 (*a*) W. Cui, P. Otten, Y. Li, K. S. Koeneman, J. Yu and R. P. Mason, *Magn. Reson. Med.*, 2004, **51**, 616; (*b*) M. Higuchi, N. Iwata, Y. Matsuba, K. Sato, K. Sasamoto and T. C. Saido, *Nat. Neurosci.*, 2005, **8**, 527; (*c*) V. D. Kodibagkar, J. Yu, L. Liu, H. P. Hetherington and R. P. Mason, *Magn. Reson. Imaging*, 2006, **24**, 959; (*d*) K. Tanaka, N. Kitamura, K. Naka and Y. Chujo, *Chem. Commun.*, 2008, 6176; (*e*) P. Porcari, S. Capuani, E. D'Amore, M. Lecce, A. La Bella, F. Fasano, R. Campanella, L. M. Migneco, F. S. Pastore and B. Maraviglia, *Phys. Med. Biol.*, 2008, **53**, 6979; (*f*) K. Tanaka, N. Kitamura, Y. Takahashi and Y. Chujo, *Bioorg. Med. Chem.*, 2009, **17**, 3818; (*g*) Y. Takaoka, T. Sakamoto, S. Tsukiji, M. Narazaki, T. Matsuda, H. Tochio, M. Shirakawa and I. Hamachi, *Nat. Chem.*, 2009, **1**, 557; (*h*) K. Tanabe, H. Harada, M. Narazaki, K. Tanaka, K. Inafuku,

H. Komatsu, T. Ito, H. Yamada, Y. Chujo, T. Matsuda, M. Hiraoka and S. Nishimoto, *J. Am. Chem. Soc.*, 2009, **131**, 15982.
9 (*a*) S. Mizukami, R. Takikawa, F. Sugihara, Y. Hori, H. Tochio, M. Wälchli, M. Shirakawa and K. Kikuchi, *J. Am. Chem. Soc.*, 2008, **130**, 794; (*b*) S. Mizukami, R. Takikawa, F. Sugihara, M. Shirakawa and K. Kikuchi, *Angew. Chem., Int. Ed.*, 2009, **48**, 3641.
10 L. Helm, *Prog. Nucl. Magn. Reson. Spectrosc.*, 2006, **49**, 45.
11 C. V. Hall, P. E. Jacob, G. M. Ringold and F. Lee, *J. Mol. Appl. Genet.*, 1983, **2**, 101.
12 (*a*) J. P. Horwitz, J. Chua, R. J. Curby, A. J. Tomson, M. A. DaRooge, B. E. Fisher, J. Mauricio and I. Klundt, *J. Med. Chem.*, 1964, **7**, 574; (*b*) A. B. Pardee, F. Jacob and J. Monod, *J. Mol. Biol.*, 1959, **1**, 165.
13 (*a*) D. Shabat, R. J. Amir, A. Gopin, N. Pessah, M. Shamis and W.-M. Dai, *Chem.–Eur. J.*, 2004, **10**, 2626; (*b*) J. A. Duimstra, F. J. Femia and T. J. Meade, *J. Am. Chem. Soc.*, 2005, **127**, 12847; (*c*) T. Komatsu, K. Kikuchi, H. Takakusa, K. Hanaoka, T. Ueno, M. Kamiya, Y. Urano and T. Nagano, *J. Am. Chem. Soc.*, 2006, **128**, 15946; (*d*) N.-H. Ho, R. Weissleder and C.-H. Tung, *ChemBioChem*, 2007, **8**, 560.
14 E. Vives, J. Schmidt and A. Pelegrin, *Biochim. Biophys. Acta*, 2008, **1786**, 126.

CHEMISTRY
A EUROPEAN JOURNAL

DOI: 10.1002/chem.201100973

Intracellular Protein Labeling with Prodrug-Like Probes Using a Mutant β-Lactamase Tag

Shuji Watanabe,[a] Shin Mizukami,[a, b] Yuri Akimoto,[a] Yuichiro Hori,[a] and Kazuya Kikuchi*[a, b]

Abstract: Intracellular protein labeling with small molecular probes that do not require a washing step for the removal of excess probe is greatly desired for real-time investigation of protein dynamics in living cells. Successful labeling of proteins on the cell membrane has been performed using mutant β-lactamase tag (BL-tag) technology. In the present study, intracellular protein labeling with novel cell membrane permeable probes based on β-lactam prodrugs is described. The prodrug-based probes quickly permeated the plasma membranes of living mammalian cells, and efficiently labeled intracellular proteins at low probe concentrations. Because these cell-permeable probes were activated only inside cells, simultaneous discriminative labeling of intracellular and cell surface BL-tag fusion proteins was attained by using cell-permeable and impermeable probes. Thus, this technology enables adequate discrimination of the location of proteins labeled with the same protein tag, in conjunction with different color probes, by dual-color fluorescence. Moreover, the combination of BL-tag technology and the prodrug-based probes enabled the labeling of target proteins without requiring a washing step, owing to the efficient entry of probes into cells and the fast covalent labeling achieved with BL-tag technology after bioactivation. This prodrug-based probe design strategy for BL-tags provides a simple experimental procedure with application to cellular studies with the additional advantage of reduced stress to living cells.

Keywords: fluorescent probes · microscopy · prodrugs · protein labeling · β-lactamase

Introduction

The specific labeling of proteins using small molecule probes has attracted much attention for the investigation of protein structure, function, localization, and protein–protein interactions.[1] The modification of target proteins with small molecules such as near-infrared fluorophores, biofunctional molecules such as biotin, and magnetic resonance imaging (MRI) agents enables a wider range of functional studies than those achieved with fluorescent proteins (FPs). Various labeling methods have been developed based on enzyme-catalyzed modification,[2] specific chelation of fluorescent ligands to short peptides,[3] and self-labeling protein tags.[4] Several reported labeling methods however, are restricted to labeling of cell surface proteins because of the cell impermeability of labeling probes or the presence of endogenous counterparts within cells.[5]

We recently described a novel method for the highly specific labeling of proteins by exploiting a mutant of 29 kDa TEM-1 β-lactamase.[6] TEM-1 efficiently hydrolyzes β-lactam derivatives and affords the corresponding hydrolysates.[7] During enzymatic hydrolysis by a wild-type TEM-1, Ser70 in the active site of the enzyme attacks the β-lactam carbonyl carbon and the nucleophilic substitution produces the acyl–enzyme intermediate. Subsequently, the acyl–enzyme intermediate is hydrolyzed by water molecules activated by a proximate carboxylate anion of Glu166. Prior studies in the E166N mutant showed that the acyl–enzyme intermediates remain stable. The labeling system involves covalent modification of the mutant TEM-1 (BL-tag) with the fluorescent β-lactam derivatives (Scheme 1a). Because these β-lactam derivatives have a carboxylate within their structure, they intrinsically show reduced transmembrane permeability.

For the intracellular application of the BL-tag technology, we focused on the prodrugs of β-lactam antibiotics that are based on the modification of carboxylic acids to noncharged ester derivatives. Prodrugs are commonly designed to improve oral bioavailability compared with the parent drugs.[8] The absorption, stability, and toxicity of the prodrugs have been rigorously investigated through rational molecular design. Although the esterified β-lactam prodrugs are inactive to β-lactamases,[9] the ester group of the prodrug is

[a] S. Watanabe, Dr. S. Mizukami, Y. Akimoto, Dr. Y. Hori, Prof. Dr. K. Kikuchi
Division of Advanced Science and Biotechnology
Graduate School of Engineering, Osaka University
2–1 Yamadaoka, Suita, Osaka 565-0871 (Japan)
Fax: (+81) 6-6879-7875
E-mail: kkikuchi@mls.eng.osaka-u.ac.jp

[b] Dr. S. Mizukami, Prof. Dr. K. Kikuchi
Immunology Frontier Research Center (IFReC), Osaka University,
3–1 Yamadaoka, Suita, Osaka 565-0871 (Japan)

Supporting information for this article is available on the WWW under http://dx.doi.org/10.1002/chem.201100973.

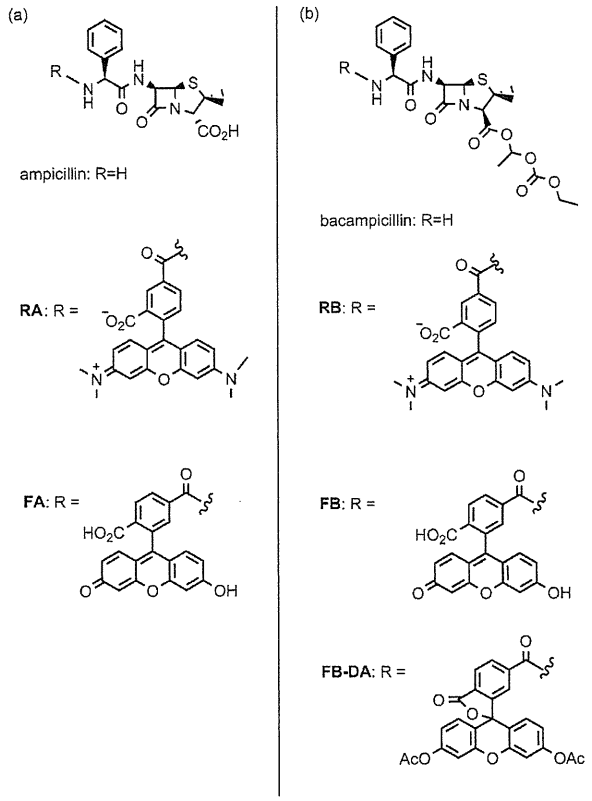

Scheme 1. Structures of a) reported ampicillin-based probes (**RA** and **FA**) and b) newly synthesized bacampicillin-based probes (**RB**, **FB**, and **FB-DA**) for BL-tag.

quickly converted into a carboxylate by the activities of intracellular esterases, which results in the accumulation of active β-lactams in cells. Thus, the labeling properties of probes can be made dependent on location by exploiting the structure of the prodrug.

Although the intracellular application of target protein labeling has been reported previously,[3,4] washing of unreacted probes, which was a necessary step in prior work, limits the robustness of the method because it is nearly impossible to completely wash out the probes in the cytoplasm. We assumed that this drawback was due to both the low efficiency of the membrane permeation and the low efficiency of the reaction with the target protein. The BL-tag technology enables simple and wide variations of probe design. In addition, BL-tag technology results in high reaction efficiency due to the use of mutated proteins that do not limit substrate entrance. Therefore, efficient delivery of the probe to the intracellular target protein allows its specific labeling without the requirement for a washing step. On the basis of these requirements, we investigated the development of probes designed for effective transport into cells using our BL-tag technology.

The present study describes a novel design strategy for cell-permeable probes for BL-tag technology based on the use of a clinical β-lactam prodrug. These bioactivation-process-based probes enabled the discrimination between same tag proteins in different locations using dual-color fluorescence. Moreover, specific labeling of intracellular target proteins without the required washing of excess probe was achieved based on the fast permeation and accumulation of labeling probes.

Results and Discussion

Design and synthesis of cell-permeable probes based on β-lactam prodrug structures: Three representative ampicillin esters (bacampicillin, pivampicillin, and talampicillin) have been well studied for their bioavailability among the clinical prodrugs of ampicillin (Scheme 1).[10] The carboxy groups of these prodrugs are converted into noncharged and lipophilic ester groups to increase the bioavailability of ampicillin. We chose bacampicillin as the core structure for the cell-permeable labeling probes because among the studied prodrugs, bacampicillin shows the best absorption by the body and is stable at neutral pH,[11] as well as being industrially available.[12] Although bacampicillin itself exhibits low antibacterial activity, once it is transformed into ampicillin by the bioactivation process, it shows high antibacterial activity (Scheme 1).[13]

The bacampicillin-based probes **RB**, **FB**, and **FB-DA** (Scheme 1b) were designed and synthesized as described in the Supporting Information (see Scheme S1). **RB** and **FB**, which are fluorophore-attached bacampicillin derivatives, were synthesized in one step by a condensation reaction of bacampicillin hydrochloride with the activated ester of the corresponding fluorophores. **FB-DA** is the diacetylated counterpart of **FB** designed for increased cell permeability. Absorption and emission spectra of the synthesized probes are shown in Figure S1 in the Supporting Information section. The fluorescence quantum yields of **RB** and **FB** were 0.50 and 0.55, respectively. Therefore, the esterification of the carboxy group of ampicillin has almost no effect on the spectroscopic properties of the conjugated fluorophore. Although **FB-DA** showed no fluorescence, this is a known characteristic of diacetylated fluorescein derivatives.[14]

The in vitro enzymatic conversion of the bacampicillin moiety to the ampicillin moiety of the synthesized probes was confirmed. HPLC and ESI-TOF MS analyses of the reaction mixture of **RB** with an esterase demonstrated the complete conversion of **RB** into **RA** (Figure S2 in Supporting Information), which specifically labels BL-tag fusion proteins.[6b] The addition of an esterase shifted the retention time of **RB**, resulting in a new peak with the same *m/z* value ($[M+H]^+$: 762.3) as that of **RA** in the MS analysis.

Specific labeling of intracellular BL-tag fusion proteins with bacampicillin-based probes: The newly synthesized probes were used for intracellular protein labeling using BL-tag technology (Scheme 2). In *E. coli*, the unmodified coding region of β-lactamase contains a signal peptide sequence for secretion into the periplasm.[15] To generate an intracellular

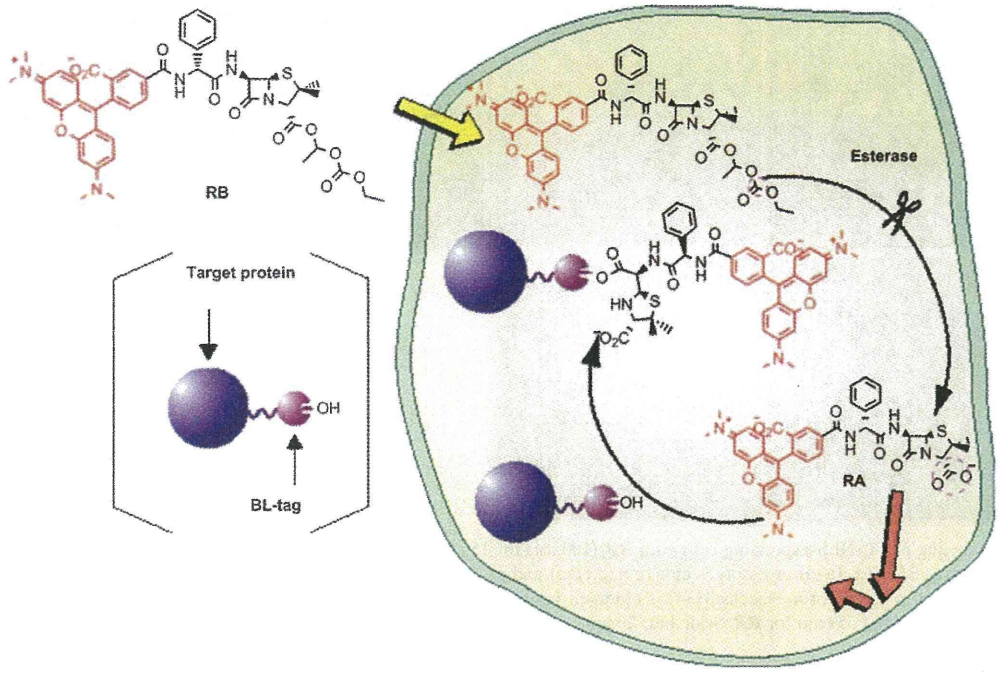

Scheme 2. Labeling mechanism of the intracellular BL-tag fusion proteins by **RB**.

form of BL proteins, the bacterial signal sequence was removed and replaced by an initiator methionine (cytoplasmic-BL).[16] To enhance expression levels, a consensus sequence for optimal translation efficiency in eukaryotes[17] was added adjacent to the initiator codon. Furthermore, to facilitate the detection of the fluorescent label, we designed BL-NLS, which is a nuclear localized BL protein, by fusing the BL-tag to three consecutive simian virus 40 (SV40) large T antigen nuclear localization sequences (NLS).[18] The intracellular expression of cytoplasmic-BL and BL-NLS were confirmed by western blot analysis (see the Supporting Information, Figure S3). Lysates of cells transfected with cytoplasmic-BL plasmids were probed with an anti-β-lactamase antibody, which revealed one major band with a molecular weight of about 25 kDa, corresponding to a cytoplasmic-BL fusion protein (see the Supporting Information, Figure S3 A; lane 1). A single band was also detected in cells transfected with BL-NLS (see the Supporting Information, Figure S3 A; lane 2). This band appeared in a slightly higher position than that of cytoplasmic-BL, which is consistent with the increase in molecular weight due to the fusion of three consecutive NLS.

HEK293T cells transfected with a vector expressing cytoplasmic-BL or BL-NLS were incubated with **RB** at a lower concentration (100 nM) than labeling probes in reported methods.[3,4] After the washing step, red fluorescence was uniformly observed in cytoplasmic-BL-expressing cells (Figure 1). In BL-NLS-expressing cells, strong red fluorescence was detected at the cell center (Figure 2 a), and the nuclear localization of the fluorescently labeled proteins was confirmed by co-staining with Hoechst 33342, which binds

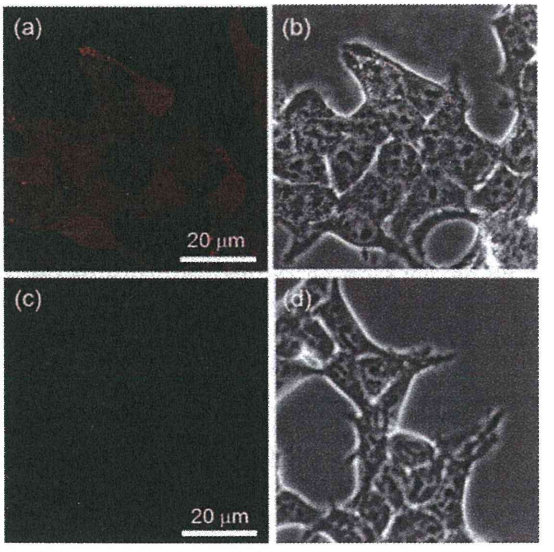

Figure 1. Specific labeling of cytoplasmic-BL-expressing cells with **RB** (100 nM) for 15 min. HEK293T cells were transfected with a plasmid encoding (a) and cytoplasmic-BL (b) or empty vector (c and d). a) and c) Fluorescence images. b) and d) Phase contrast images. For fluorescence microscopic images, the cells were excited at 559 nm. Scale bar: 20 μm.

to DNA in the nucleus (Figure 2 d). The merged fluorescence image indicates the specific labeling of BL-NLS by **RB**. Nonspecific accumulation of **RB** in **RB**-treated cells was not observed, despite the fact that rhodamine-based fluorescent probes often show nonspecific accumulation in organelles such as mitochondria owing to their positive charge

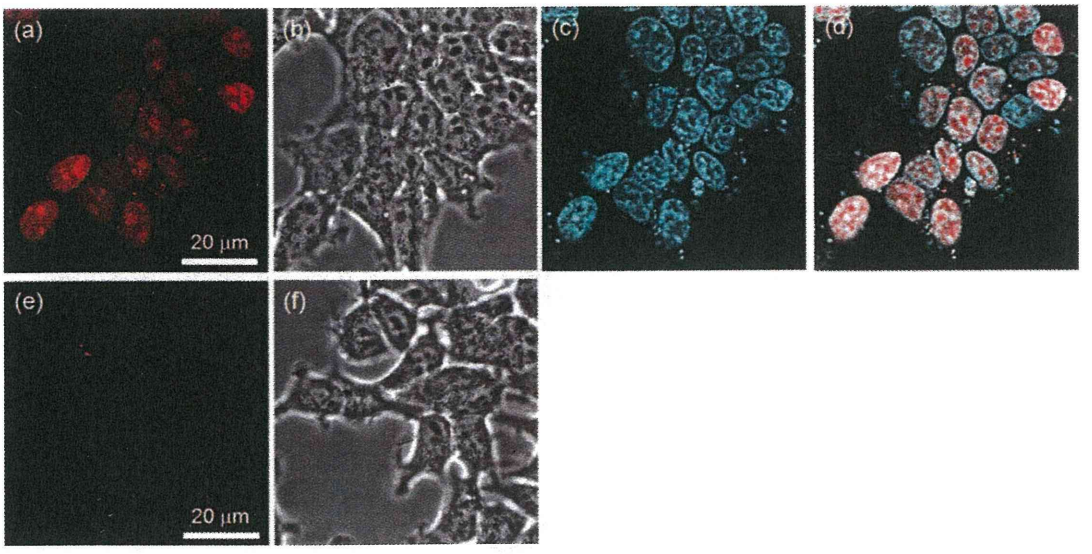

Figure 2. Specific labeling of BL-NLS-expressing cells with **RB** (100 nM) for 15 min and co-stained with Hoechst33342. HEK293T cells were transfected with a plasmid encoding BL-NLS (a–d) or empty vector (e and f). a) and e) Fluorescence images of a channel for **RB**. b) and f) Phase contrast images. c) Fluorescence images of a channel for Hoechst33342. d) Merged image of a) and c). For fluorescence microscopic images, the cells were excited at 405 nm for Hoechst33342 and at 559 nm for **RB**. Scale bar: 20 μm.

and hydrophobicity. Rhodamine derivatives are therefore often used as probes for mitochondria.[19] When cells expressing BL-NLS were incubated with high concentrations of **RA** (5 μM), no staining of the cell nuclei was observed (see the Supporting Information, Figure S4). The intracellular labeling experiments suggested that the cell permeability of the labeling probe would be largely improved by introducing a bacampicillin structure into the probe design.

Subsequently, labeling of BL-NLS fusion proteins with **FB** or **FB-DA** was attempted using the same concentration (100 nM) as for **RB**. Incubation of cells expressing BL-NLS with **FB** did not show fluorescence in the nuclei (Figure 3a and 3b). On the other hand, nuclei of cells treated with **FB-DA** showed strong green fluorescent signals (Figure 3c and 3d). These results indicate that the cell permeability of BL-tag labeling probes depends on not only the carboxy group of the β-lactam substrates but also on the structure of the fluorophores. **FB-DA** showed sufficient cell permeability because the anionic groups of the fluorescein moiety are wholly acetylated.

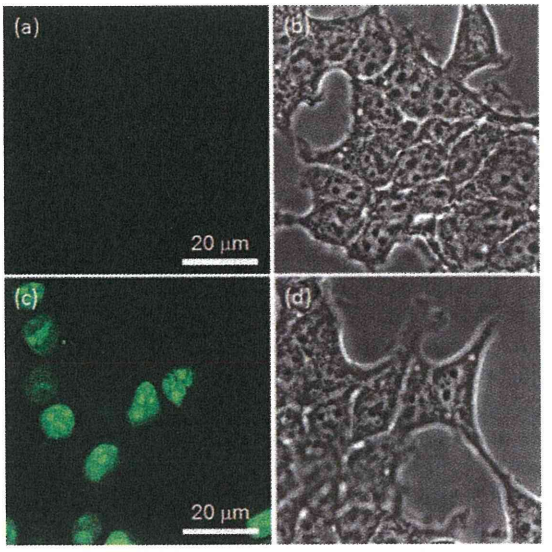

Figure 3. Specific labeling of BL-NLS-expressing cells with **FB** (100 nM) (a and b) or **FB-DA** (100 nM) (c and d) for 15 min. HEK293T cells were transfected with a plasmid encoding BL-NLS. a) and c) Fluorescence images. b) and d) Phase contrast images. For fluorescence microscopic images, the cells were excited at 473 nm. Scale bar: 20 μm.

Simultaneous and discriminative labeling of BL-tag fusion proteins localized at the cell surface and intracellular regions: A unique application of prodrug-based labeling technology, namely the simultaneous discriminative labeling of BL-tag fusion proteins localized at the cell surface and intracellular regions, was demonstrated (Scheme 3). The ability to discriminate between membrane proteins and intracellular proteins in the same cell is critical for the understanding of protein trafficking.[20] Protein labeling methods use cell-permeable probes for intracellular protein labeling that are also recognized by the target proteins on the cell surface. Therefore, to perform discriminative labeling with a single tag, the extracellular target proteins need to be blocked with cell-impermeable probes to allow specific labeling of intracellular proteins by cell-permeable probes.

In the present experiments, the tag recognition ability of bacampicillin-based labeling probes was expected to be largely suppressed before esterase-mediated hydrolysis. Because esterified benzylpenicillin is a very poor substrate for class A β-lactamases,[9] a negatively charged substituent on the substrate is essential for the recognition by β-lacta-

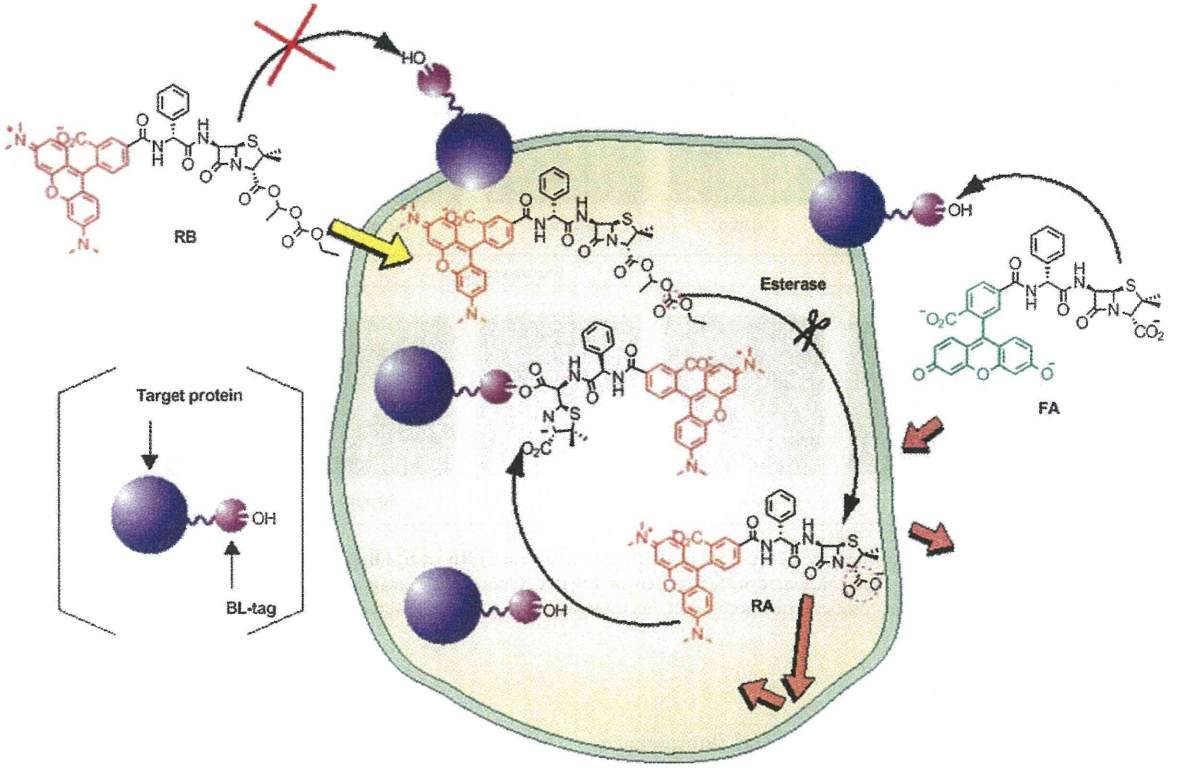

Scheme 3. Simultaneous discriminative labeling mechanism of the intracellular and cell surface BL-tag fusion proteins by using **RB** and **FA**.

mase.[21] Purified BL-tag proteins (10 μM) were incubated with **RA** (12 μM), **FA** (12 μM), or **RB** (100 μM) in 100 mM HEPES buffer (pH 7.4) at 25 °C. The reaction mixtures were sampled at various time points and analyzed by SDS-PAGE (Figure S5 in Supporting Information). The fluorescently labeled proteins were detected by irradiating the gels with UV light. A time course of fluorescent band signals was used to evaluate the labeling reaction rates of the three probes with the BL-tag protein. The in vitro reaction of the BL-tag protein with **RB** was significantly slower than that of **FA** and **RA**, even in the presence of excess amount of substrates. Hence, ampicillin-based probes such as **RA** and **FA** preferentially react with extracellular BL-tag fusion proteins compared with bacampicilin-based probes such as **RB** and **FB-DA**.

The two kinds of fusion proteins, BL-NLS and BL-EGFR, were used for the simultaneous labeling experiment. BL-EGFR is the result of the fusion of the BL-tag with epidermal growth factor receptor (EGFR). We previously succeeded in labeling cell surface BL-EGFR with ampicillin-based labeling probes.[6b] HEK293T cells co-expressing BL-NLS and BL-EGFR were incubated with **RB** (100 nM) and **FA** (100 nM) simultaneously, and then washed before imaging with a confocal fluorescence microscope. As shown in Figure 4, green fluorescence corresponding to **FA** was observed along the plasma membranes and red fluorescence corresponding to **RB** was observed in the nuclei. The present results demonstrate the successful selective labeling of intracellular and membrane proteins with two different colored fluorophores by using the same tag.

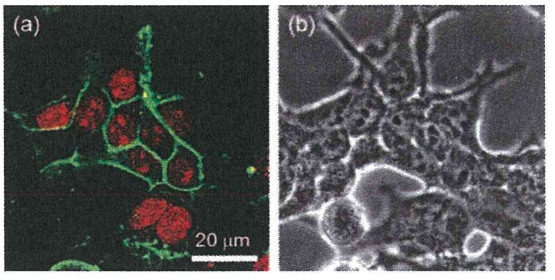

Figure 4. Simultaneous labeling of BL-tag fusion proteins localized at the cell membrane and nucleus. HEK293T cells were transfected with two kinds of plasmids encoding BL-NLS and BL-EGFR, and labeled with **RB** (100 nM) and **FA** (100 nM) for 15 min. a) Fluorescence merged image of labeled cells. b) Phase contrast image. For fluorescence microscopic images, the cells were excited at 473 nm for **FA** and 559 nm for **RB**. Scale bar: 20 μm.

Fluorescence labeling of BL-NLS proteins without washing procedure: Finally, time-lapse imaging of BL-NLS fusion proteins, fluorescently labeled with **RB** or **FB-DA**, was carried out using low probe concentrations. Surprisingly, a decrease in the concentration of the probe to 5 nM resulted in the detection of specific protein labeling within a 30 min period without a washing procedure (Figure 5, and Supplementary movies S1 and S2 in Supporting Information). This

